Title: Cisplatin drives mitochondrial dysregulation in sensory hair cells

David S. Lee[1], Angela Schrader[1], Jiaoxia Zou[2], Wee Han Ang [2,3], Mark E. Warchol[1,4], and Lavinia Sheets[1,5]

[1] Department of Otolaryngology – Head and Neck Surgery, Washington University School of Medicine, St. Louis, MO 63110 USA

[2] Department of Chemistry, National University of Singapore, Singapore 117543, Singapore

[3] NUS Graduate School – Integrated Science and Engineering Programme (ISEP), National University of Singapore, Singapore 119077, Singapore

[4] Department of Neuroscience, Washington University School of Medicine, St. Louis, MO 63110 USA

[5] Department of Developmental Biology, Washington University School of Medicine, St. Louis, MO 63110 USA

Conflicts of Interests: The authors have declared that no conflict of interest exists.

Corresponding Author: Lavinia Sheets, PhD
Washington University School of Medicine
Department of Otolaryngology—Head & Neck Surgery
660 S. Euclid Ave. Campus Box 8115
St. Louis, MO 63110
Phone: +1 (314) 273-1857 Fax: +1 (314) 453-0489
Email: sheetsl@wustl.edu

Abstract:

Cisplatin is a commonly used chemotherapy that causes permanent hearing loss by injuring cochlear hair cells. The underlying mechanisms that drive hair cell loss remain unknown, but mitochondria have emerged as potential mediators of cisplatin ototoxicity. Direct observation of changes in hair cell mitochondrial function are challenging because the mammalian inner ear is optically inaccessible. Here, we perform live *in vivo* imaging of hair cells within the zebrafish lateral-line organ to evaluate the role of mitochondria in cisplatin ototoxicity. Using a genetically encoded biosensor that measures cumulative mitochondrial activity in hair cells, we demonstrate that greater redox history increases susceptibility to cisplatin. Next, we conduct time-lapse imaging of individual hair cells to understand dynamic changes in mitochondrial homeostasis. We observe spikes in mitochondrial calcium and cytosolic calcium immediately prior to hair cell death. Furthermore, we use a mitochondrially-localized probe that fluoresces in the presence of cisplatin to show that cisplatin accumulates in hair cell mitochondria. Lastly, we demonstrate that this accumulation occurs before mitochondrial dysregulation, Caspase-3 activation, and ultimately, hair cell death. Our findings provide additional evidence that suggest mitochondria are integral to cisplatin ototoxicity and cisplatin directly targets hair cell mitochondria.

Key Words: cisplatin ototoxicity, zebrafish, mitochondria, *in vivo* imaging

43 **Introduction:**

44 Cisplatin is a commonly used and effective chemotherapy for the management of solid
45 tumors, but also causes irreversible hearing loss in more than 50% of treated adults and
46 children (1-3). This hearing loss decreases quality of life and has additional long-term
47 ramifications in children for its effect on speech and language development (4-6).
48 Cisplatin has been used clinically since the 1970s and numerous candidate therapies
49 have been developed in an effort to reduce or eliminate cisplatin ototoxicity (7).
50 However, only one therapy has been approved by the United States Food and Drug
51 Administration to mitigate cisplatin-induced hearing loss and its use is limited to children
52 with localized non-metastatic solid tumors; otoprotective drug candidates for adults
53 remain investigational (8). Drug discovery has been challenged, in part, by an
54 incomplete understanding of the cellular mechanisms that drive cisplatin-induced
55 hearing loss. Therefore, elucidating the pathophysiology of cisplatin ototoxicity may
56 have substantial clinical implications.

57

58 Cisplatin causes damage to cochlear hair cells, the sensory receptors that facilitate
59 hearing, and may do so through a variety of mechanisms. The most studied pathway of
60 cisplatin cytotoxicity is the formation of bulky adducts with nuclear DNA, thereby
61 preventing replication in rapidly dividing cells, such as cancer cells (9-11). Yet, hair cells
62 are mitotically inactive, which suggests that another process may drive their vulnerability
63 to cisplatin. More recently, production of pathologic reactive oxygen species (ROS) has
64 been shown to facilitate cisplatin ototoxicity, suggesting that free radical scavengers
65 might mitigate this process (12, 13). Although multiple pathways may lead to ROS

66 overproduction, mitochondria have emerged as likely mediators of cisplatin ototoxicity
67 because they are a major source of physiologic ROS and represent the only other
68 organelle in hair cells to contain DNA (14, 15). In support of this theory, preclinical
69 studies show that cisplatin leads to elevated mitochondrial ROS production, increased
70 ratios of Bax to Bcl-2 (mediators of apoptosis and hair cell survival, respectively), and
71 activated Caspase-3 in hair cells (16-18).
72
73 The pattern of cochlear injury in response to cisplatin further implicates mitochondria as
74 critical players in cisplatin ototoxicity. The cochlea is tonotopically organized such that
75 hair cells located at its base transmit high frequencies and those present at its apex
76 transmit low frequencies (19). Cisplatin preferentially causes high-frequency hearing
77 loss by damaging hair cells at the basal turn of the cochlea (20). While the mechanisms
78 that underlie this selective hair cell susceptibility are unknown, tonotopic differences in
79 hair cell metabolic activity, endogenous levels of antioxidants, and intracellular calcium
80 homeostasis may contribute to cisplatin's distinct pattern of cochlear injury (21-23).
81 Mitochondria, the organelle responsible for many of these functions, may therefore
82 serve as direct or indirect targets of cisplatin. Similar relationships between
83 mitochondria and high-frequency hearing loss have also been observed in other
84 disease processes, including presbycusis (age-related hearing loss) and
85 aminoglycoside ototoxicity (24-27). Altogether, the literature suggests that mitochondrial
86 dysregulation is potentially a key cellular event that drives cisplatin ototoxicity.
87

88 Despite an association to ototoxicity, direct observation of cisplatin-induced
89 mitochondrial dysregulation has been elusive. The mammalian cochlea is generally not
90 suitable for live imaging because it is encased in bone and optically inaccessible. In
91 contrast, zebrafish contain hair cells that reside along their surface in a sensory organ
92 called the lateral line. These hair cells are bundled into innervated structures called
93 neuromasts, and they are genetically, morphologically, and functionally similar to
94 mammalian hair cells (28, 29). Since zebrafish larvae are transparent, their lateral-line
95 organ permits consistent drug exposure protocols and live imaging of intact hair cells.
96 These features make zebrafish a powerful model for exploring mechanisms of cisplatin
97 ototoxicity and targeted drug discovery (30, 31). In the present study, we use transgenic
98 zebrafish with genetically encoded biosensors to explore mitochondrial contributions to
99 selective hair cell susceptibility and to characterize the progression of mitochondrial
100 dysregulation after exposure to cisplatin. Pre- and post-exposure imaging demonstrate
101 that greater cumulative mitochondrial activity increases hair cell vulnerability to cisplatin.
102 Time-lapsed imaging of zebrafish treated with cisplatin demonstrates a slow rise in hair
103 cell mitochondrial calcium and cytosolic calcium followed by a rapid elevation
104 immediately prior to death. We further show that cisplatin accumulates in the
105 mitochondria, and that greater amounts of mitochondrial accumulation of cisplatin is
106 associated with hair cell death. Lastly, we demonstrate that cisplatin accumulation
107 within mitochondria occurs prior to mitochondrial dysregulation and Caspase-3
108 activation. Cumulatively, these results not only provide further evidence that hair cell
109 mitochondria are involved in cisplatin ototoxicity, but also suggest that they are direct
110 targets of cisplatin itself.

111 **Results:**

112 ***Greater cumulative mitochondrial activity in hair cells increases susceptibility to***
113 ***cisplatin***

114 As stated above, the mammalian cochlea demonstrates selective injury of hair cells in
115 high frequency regions following cisplatin exposure. We have previously observed that
116 the zebrafish lateral-line organ also experiences selective hair cell death in response to
117 cisplatin, i.e., exposure to cisplatin appears to target a subset of neuromast hair cells in
118 a dose-dependent manner (32). Since the lateral-line organ does not exhibit tonotopic
119 organization, selective hair cell injury observed within zebrafish is surprising, especially
120 when considering neuromast hair cells diffusely take up cisplatin within 15 minutes of
121 exposure (33). Our initial experiments investigate whether mitochondria play a role in
122 differential hair cell vulnerability to cisplatin.

123

124 A prior zebrafish study investigating lateral-line injury after exposure to neomycin, an
125 aminoglycoside antibiotic that also causes high-frequency hearing loss, indicates that
126 cumulative mitochondrial activity contributes to hair cell vulnerability (21). To determine
127 whether the lateral-line organ demonstrates a similar pattern of selective susceptibility in
128 response to cisplatin, we performed experiments on transgenic zebrafish expressing the
129 biosensor mitoTimer (*Tg*(*myo6b:mitoTimer*)) in their hair cells. MitoTimer encodes a
130 DsRed mutant (DsRed1-E5) localized within mitochondria that irreversibly changes from
131 green to red over time as the Tyr-67 residue undergoes dehydrogenation (34). Thus,
132 mitoTimer serves as an indicator of cumulative mitochondrial oxidation based on the
133 ratio of red to green fluorescence within individual hair cells (21, 35). We measured

134 baseline mitoTimer fluorescence in 6-day-old transgenic larvae, then exposed them to 1
135 mM cisplatin for 2 hours followed by 2 hours of recovery in embryo media (EM). This
136 protocol produces a lesion with approximately 60% hair cell death (32). Upon
137 completion of the cisplatin exposure protocol, we obtained post-treatment images and
138 classified each hair cell as alive or dead based on fragmentation and clearance from the
139 neuromast (21, 36). Baseline red:green ratios of mitoTimer fluorescence were
140 normalized to the median ratio of living hair cells. We observed a significant difference
141 in the normalized median mitoTimer fluorescence ratios between living and dying cells,
142 with dying hair cells showing higher levels of red fluorescence (Living cells: 1.00, 95%
143 confidence interval = 0.83 to 1.13, n = 113 hair cells; dying cells: 1.60, 95% confidence
144 interval = 1.51 to 1.78, n = 73 hair cells; Mann-Whitney U test, $p < 0.0001$; Figure 1A –
145 C). This result suggests that greater cumulative mitochondrial activity increases
146 vulnerability to cisplatin-induced hair cell death.
147
148 To verify this observation, we sought to determine whether elevating baseline
149 mitochondrial activity prior to cisplatin exposure affects hair cell vulnerability. Therefore,
150 we exposed 5-day-old *Tg*(*myo6b:mitoTimer*) larvae to either continuous water flow in a
151 microflume apparatus or maintained larvae in stationary EM for 24 hours (Figure 2A).
152 We then measured red:green ratios of mitoTimer fluorescence in individual hair cells
153 and normalized values to the median ratio of control hair cells. Larvae exposed to
154 sustained water current demonstrated significantly increased red:green ratios of
155 mitoTimer fluorescence compared to those maintained in EM (flume cells: 1.54, 95%

156 confidence interval = 1.41 to 1.61, n = 466 cells; no flume cells: 95% confidence interval
157 = 0.89 to 1.12, n = 458 cells; Mann-Whitney U test, $p < 0.0001$; Figure 2 B–C, F).
158
159 After establishing that sustained mechanical stimulation increases cumulative lateral-
160 line hair cell mitochondrial activity, we then exposed fish to either media exchange or
161 250 μM cisplatin for 2 hours followed by 4 hours of recovery in EM (Figure 2A). This
162 protocol produces approximately 30% hair cell death (32). Upon conclusion of the
163 cisplatin exposure protocol, we obtained post-treatment images and counted the
164 number of remaining hair cells in each neuromast compared to baseline (Figure 2, B-
165 G). While all neuromasts exposed to cisplatin demonstrated a decreased mean
166 percentage of viable hair cells when compared to control neuromasts, those that were
167 also exposed to sustained mechanical stimulation exhibited a significantly lower mean
168 percentage of surviving hair cells relative to neuromasts in fish not exposed to sustained
169 water current (Media exchange-no flume: 96.7%, 95% confidence interval = 91.7% to
170 98.2%, n = 18 neuromasts; media exchange-flume: 97.5%, 95% confidence interval =
171 94.4% to 100%, n = 17 neuromasts; cisplatin-no flume: 72.1%, 95% confidence interval
172 = 66.6% to 77.7%, n = 18 neuromasts; cisplatin-flume: 55.1%, 95% confidence interval
173 = 44.3% to 65.8%, n = 18 neuromasts; Tukey's multiple comparisons test, adjusted ns =
174 0.94, **adjusted $p = 0.0012$, ****adjusted $p < 0.0001$; Figure 2G). These results indicate
175 that greater cumulative mitochondrial activity increases hair cell vulnerability to cisplatin.
176
177

178 ***Influx of mitochondrial calcium precedes hair cell death following cisplatin***
179 ***exposure***

180 Mitochondria have been implicated in cisplatin cytotoxicity as sources of pathologic
181 ROS and initiators of Caspase-3-mediated apoptosis in both cancer and non-cancer
182 models (16-18, 37, 38). However, the cellular events and time course of mitochondrial
183 dysregulation have not been well characterized. Our next set of experiments use live *in*
184 *vivo* imaging of transgenic zebrafish with genetically encoded biosensors to investigate
185 the time course of cisplatin-induced mitochondrial dysregulation.
186
187 Mitochondria play a key role in intracellular calcium homeostasis (39). We therefore
188 evaluated the time course of changes in mitochondrial calcium levels in response to
189 cisplatin. These experiments utilized transgenic zebrafish that stably express calcium
190 indicator, GCaMP3, in the mitochondria of their hair cells (*Tg(myo6b:mitoGCaMP3);*
191 *(36)).* We exposed transgenic larvae at 5 – 7 days post-fertilization (dpf) to either media
192 exchange or 1 mM cisplatin for 2 hours and then allowed recovery in EM for an
193 additional 2 hours. Baseline mitoGCaMP3 fluorescence was measured before treatment
194 initiation and images were acquired every 10 minutes throughout the duration of the
195 cisplatin exposure protocol (Figure 3A). We then determined the change in
196 mitoGCaMP3 fluorescence relative to baseline ($\Delta F/F_o$) of individual hair cells at each
197 time point. Next, we classified cells as dead or alive based on their pattern of hair cell
198 mitochondrial fragmentation and extrusion. We aligned data to the time at which dying
199 hair cells were cleared from the neuromast (Figure 3B–D). All cisplatin-exposed hair
200 cells demonstrated a slight elevation in mitochondrial calcium levels compared to those

201 that underwent media exchange alone (control). However, dying hair cells exhibited a
202 gradual elevation of mitochondrial calcium that peaked immediately prior to hair cell
203 death (Figure 3D). This phenomenon was not observed in living or control hair cells.
204 When evaluating peak changes in mitochondrial calcium levels, the median change in
205 fluorescence of hair cells normalized to controls was significantly greater among dying
206 hair cells than living or control hair cells (control cells: 1.00, 95% confidence interval =
207 0.97 to 1.05, n = 233 cells; alive cells: 1.89, 95% confidence interval = 1.62 to 2.09, n =
208 136 cells; dead cells: 3.51, 95% confidence interval = 3.20 to 3.82, n = 155; Dunn's
209 multiple comparisons test, ****adjusted $p < 0.0001$; Figure 3E). To evaluate when
210 surges in mitochondrial calcium levels occurred, we measured the time at which half the
211 maximum change in fluorescence was observed ($t_{1/2}$ maximum $\Delta F/F_O$) relative to
212 neuromast clearance. This occurred, on average, 36.3 minutes prior to hair cell
213 fragmentation (95% confidence interval = 32.9 to 39.6 minutes, Table 1). Altogether,
214 these data suggest that cisplatin leads to a slow accumulation of hair cell mitochondrial
215 calcium followed by a rapid elevation immediately prior to death.
216

217 ***Calcium accumulates in cytosol of dying hair cells after exposure to cisplatin***

218 We next explored the time course of cytosolic calcium shifts in response to cisplatin.
219 These experiments utilized transgenic zebrafish that express GCaMP3 in the cytosol of
220 hair cells (*Tg(myo6b:cytoGCaMP3); (36)*). We measured baseline cytoGCaMP3
221 fluorescence of transgenic larvae at 5 – 7 dpf, exposed them to either media exchange
222 or 1 mM cisplatin followed by 2 hours of recovery in EM, and obtained time-lapse
223 images at 10-minute intervals (Figure 4A–B). The $\Delta F/F_O$ of individual hair cells at each

224 time point was determined and these changes in fluorescence were aligned to time of
225 neuromast clearance (Figure 4C). Among dying hair cells, we observed a slow rise in
226 cytosolic calcium levels followed by a sharp peak immediately before fragmentation.
227 Similar to the observed surge of mitochondrial calcium in dying hair cells (Figure 3),
228 large shifts in cytosolic calcium were not observed in control or living hair cells. The
229 median change in maximum fluorescence over baseline (normalized to controls) was
230 significantly greater among dying hair cells than living or control hair cells (control cells:
231 1.00, 95% confidence interval = 0.98 to 1.01, n = 169 cells; alive cells: 1.17, 95%
232 confidence interval = 1.12 to 1.23, n = 155 cells; dead cells: 1.70, 95% confidence
233 interval = 1.40 to 1.87, n = 87 cells; Dunn's multiple comparisons test, ****adjusted $p <$
234 0.0001; Figure 4D). The $t_{1/2}$ maximum $\Delta F/F_O$ of cytoGCaMP3 occurred 24.9 minutes
235 prior to clearance from the neuromast (95% confidence interval = 22.5 to 27.4 minutes,
236 Table 1). This shift in cytosolic calcium took place 11.3 minutes after the accumulation
237 of mitochondrial calcium (95% confidence interval = 5.9 to 16.7 minutes, Tukey's
238 multiple comparisons, ****adjusted $p < 0.0001$, Table 1). These data suggest that dying
239 hair cells experience a large increase in cytosolic calcium levels shortly after surges in
240 mitochondrial calcium levels.
241

242 ***Cisplatin treatment leads to progressive activation of Caspase-3 prior to hair cell***
243 ***death***

244 We have previously shown that cisplatin induces Caspase-3-mediated apoptosis in
245 conjunction with disruption of hair cell mitochondrial bioenergetics, suggesting a
246 mitochondrially driven cell death pathway (18). To evaluate the onset and pattern of

247 Caspase-3 activation, we exposed wildtype larvae at 6 dpf to either media exchange or
248 1 mM cisplatin for 2 hours, then allowed recovery in EM for an additional 2 hours. At
249 baseline and every 30-minute interval, a subset of larvae was euthanized, fixed, and
250 stained for activated Caspase-3 (Figure 5A–B). We quantified the percentage of hair
251 cells with activated Caspase-3 present within a given neuromast at each time point. We
252 then averaged these percentages within each larva to account for fish-to-fish variability
253 in response to cisplatin. Cisplatin-exposed larvae demonstrated significantly greater
254 percentages of hair cells with activated Caspase-3 than control fish at approximately 90
255 minutes after treatment (Figure 5C, mixed model, Bonferroni's multiple comparisons
256 test, *adjusted $p = 0.016$, **adjusted $p = 0.0012$, ****adjusted $p < 0.0001$; n = 42 – 45
257 neuromasts per time point from 14 – 15 fish; Table 2). These results indicate that
258 activation of Caspase-3-mediated apoptosis begins in a subset of hair cells within 90
259 minutes of 1 mM cisplatin treatment and peaks at ~210 minutes after initiating the
260 treatment protocol. Cumulatively, these observations suggest activation of the intrinsic
261 apoptosis pathway precedes mitochondrial dysfunction and subsequent hair cell death.
262

263 ***Cisplatin heterogeneously accumulates in hair cell mitochondria prior to***
264 ***mitochondrial dysregulation and Caspase-3 activation***

265 The prior time-lapse imaging experiments demonstrate that rapid mitochondrial
266 dysfunction occurs prior to hair cell death. This dysfunction may occur due to a variety
267 of reasons, like disrupted endoplasmic reticulum calcium shuttling or ROS
268 overproduction (24, 27, 40). Yet to be determined was whether hair cell mitochondria
269 are direct targets of cisplatin or if mitochondrial dysregulation is purely collateral

270 damage from different cellular processes. Prior literature indicates that cisplatin
271 accumulates in the mitochondria of cancer cell lines, presumably exerting its anticancer
272 effects through adduct formation with mitochondrial DNA (41). Yet, cisplatin
273 accumulation in mitochondria had not been demonstrated within hair cells. We therefore
274 used Rho-Mito, a mitochondria-targeting probe that fluoresces when bound to cisplatin,
275 to explore the uptake of cisplatin in hair cell mitochondria of live zebrafish (41). To
276 identify the location of mitochondria, we used the transgenic zebrafish reporter line
277 t*g(myo6b:mitoGCaMP3)* ((36); see Figure 3). We exposed larvae at 5 – 7 dpf to either
278 media exchange or 1 mM cisplatin for 1 hour, then incubated them in Rho-Mito 3 μM for
279 15 minutes. Next, baseline images were acquired at this time to observe overlap
280 between Rho-Mito and mitoGCaMP3 fluorescence. The larvae were then allowed to
281 recover for an additional 4 hours in EM. We obtained post-treatment images at the
282 conclusion of the cisplatin exposure protocol and classified each hair cell as alive or
283 dead as previously described (21, 36). Baseline fluorescence of Rho-Mito was
284 normalized to the median of living hair cells. We first noticed that strong Rho-Mito
285 fluorescence overlaps with mitoGCaMP3 in a subset of hair cells present within a given
286 neuromast (Figure 6A – C). This overlap indicates that hair cell mitochondria
287 accumulate cisplatin. Furthermore, hair cells that died following 4 hours recovery
288 demonstrated a significantly higher amount of Rho-Mito fluorescence than hair cells that
289 lived (Dead cells: 2.51, 95% confidence interval = 1.82 to 4.08, n = 92 hair cells; living
290 cells: 1.00, 95% confidence interval = 0.93 to 1.08, n = 229 hair cells; Mann-Whitney U
291 test, $p < 0.0001$; Figure 6D – E). We also observed differences in mitochondrial calcium
292 levels within individual hair cells 1 hour following exposure to cisplatin. However,

293 observed differences in mitochondrial calcium levels at this timepoint did not correlate
294 with cisplatin ototoxicity (Mann-Whitney U test, ns = 0.14; Figure 6F). This result is
295 consistent with what we reported in Figure 4C, where we observed heterogeneous
296 mitoGCaMP3 fluorescence in individual hair cells at baseline, and minimal changes in
297 mitochondrial calcium following 60 minutes cisplatin exposure. These data reveal that
298 mitochondrial accumulation of cisplatin corresponds with hair cells that subsequently die
299 following cisplatin exposure.
300
301 A previous study using fluorescently labeled cisplatin suggests diffuse uptake into hair
302 cells within 15 minutes following exposure (33). To confirm heterogeneous
303 accumulation of cisplatin in mitochondria and explore the time course of mitochondrial
304 localization, we performed a follow-up experiment in transgenic zebrafish that do not
305 express a reporter in mitochondria to ensure that Rho-Mito localization in mitochondria
306 was not influenced by mitoGCaMP3. We used transgenic fish expressing GFP in
307 neuromast supporting cells to provide a silhouette of hair cells as previously described
308 (*Tg(TNKS1bp1:EGFP);* (18, 42, 43)). We exposed 5 – 7 dpf larvae to 1 mM cisplatin for
309 various lengths of time, incubated them in 3 μM Rho-Mito, then acquired images (Figure
310 7A-C). Rho-Mito fluorescence of each hair cell was normalized to the median of control
311 hair cells that were incubated in EM alone (Figure 7A). Neuromast hair cells exposed to
312 cisplatin demonstrated significantly greater Rho-Mito fluorescence compared to control
313 (Control hair cells: 1.00, 95% confidence interval = 0.95 to 1.05, n = 287 hair cells; 30-
314 minute exposure: 1.44, 95% confidence interval = 1.27 to 1.77, n = 337 hair cells; 60-
315 minute exposure: 1.76, 95% confidence interval = 1.50 to 2.09, n = 320 hair cells;

316 Dunn's multiple comparisons test, ****adjusted $p < 0.0001$; Figure 7D). Neuromast
317 exposed to cisplatin demonstrated heterogeneous mitochondrial accumulation, with a
318 subset of hair cells accumulating cisplatin within their mitochondria (Figure 7B-C). On
319 post-hoc analysis, hair cells incubated in cisplatin for 60 minutes did not demonstrate
320 increased accumulation of Rho-Mito fluorescence compared to those incubated for only
321 30 minutes (Dunn's multiple comparisons test, adjusted ns > 0.9999; Figure 7D). Since
322 Caspase-3 activation is observed in a subset of hair cells ~90 minutes after onset of
323 cisplatin treatment (Figure 5), these data indicate that mitochondrial accumulation of
324 cisplatin occurs prior to events that signal hair cell death. Altogether, these data suggest
325 that 1) mitochondrial accumulation of cisplatin occurs in some, but not all, hair cells
326 within the first 30 minutes of exposure, 2) greater accumulation of mitochondrially-
327 localized cisplatin corresponds with hair cell death, and 3) mitochondrial accumulation
328 of cisplatin precedes Caspase-3 activation and mitochondrial dysregulation.
329
330 **Discussion:**
331 Our recent studies in zebrafish lateral-line hair cells provided evidence that cisplatin
332 disrupts mitochondrial homeostasis and initiates the intrinsic apoptosis pathway through
333 activation of the downstream effector Caspase-3 in zebrafish lateral-line hair cells (18).
334 In this study, we evaluated whether cumulative mitochondrial activity contributes to hair
335 cell susceptibility to cisplatin, examined the time course of hair cell calcium
336 dysregulation, and determined whether cisplatin accumulates within hair cell
337 mitochondria following exposure. These data reveal that hair cell susceptibility to
338 cisplatin-induced death correlates with both cumulative mitochondrial activity and

339 accumulation of cisplatin within mitochondria, and that mitochondrial accumulation of
340 cisplatin is an early event that precedes activation of Caspase-3. Additionally, we show
341 that mitochondrial and cytosolic calcium, which are elevated in all cisplatin treated hair
342 cells, gradually increase then surge prior to hair cell death. Taken together, these
343 results suggest that cisplatin directly targets hair cell mitochondria, and that
344 accumulation of cisplatin within hair cell mitochondria drives mitochondrial dysregulation
345 and contributes to hair cell death.
346
347 ***Cumulative hair cell mitochondrial activity may underlie selective vulnerability to***
348 ***cisplatin***

349 Our evaluation of cisplatin toxicity in the zebrafish lateral line indicates that hair cells
350 with higher cumulative metabolic activity are more vulnerable to cisplatin-induced death.
351 This observation corresponds with two recent studies evaluating susceptibility of lateral
352 line hair cells to the ototoxic antibiotic neomycin. The first study, which established and
353 validated the hair cell expressing mitoTimer transgenic line used in this study, revealed
354 that hair cells with greater cumulative mitochondrial activity were more susceptible to
355 neomycin-induced death (21). A subsequent study reported that hair cells with reduced
356 mitochondrial oxidation and ROS buildup were less vulnerable to neomycin (44). Taken
357 together, work in zebrafish lateral-line hair cells supports that cumulative oxidation of
358 mitochondria and accumulation of ROS underlies the specific susceptibility of hair cells
359 to ototoxic insults.
360

361 How does information from zebrafish lateral line studies relate to hair cell susceptibility
362 in humans? In patients that experience ototoxicity from cisplatin treatment, hearing
363 impairment manifests as high frequency hearing loss (45). This observed clinical
364 outcome is due to cisplatin preferentially affecting outer hair cells at the basal turn of
365 cochlea, corresponding to the region responsible for detection of high frequency
366 sounds. Preferential ototoxicity to hair cells at the base of the cochlea could be due to
367 unequal distribution of cisplatin within the cochlea, with higher accumulation of
368 chemotherapy at the base than apex (1, 46), and/or intrinsic vulnerability of high
369 frequency outer hair cells to cisplatin. Our results suggest differential hair cell
370 vulnerability to cisplatin is, at least in part, related to differences in mitochondrial
371 metabolism. Observations from cochlear studies in mammalian model systems support
372 this idea. High frequency outer hair cells have been shown to be metabolically more
373 responsive to their microenvironment than low frequency outer hair cells (47, 48), and
374 genetic disruption of mitochondrial bioenergetic homeostasis makes outer hair cells
375 more susceptible to cisplatin-induced death (49, 50).
376

377 ***Hair cell ability to regulate intracellular calcium homeostasis may be predictive of***
378 ***vulnerability to cisplatin***

379 Intracellular calcium homeostasis may contribute to hair cell susceptibility to
380 environmental and ototoxic insults (51). Mitochondria play a critical role in regulating
381 local intracellular calcium concentrations as well as provide ATP to drive clearance of
382 cytosolic Ca^{2+} via plasma membrane Ca^{2+}-ATPases (PMCA1 & PMCA2a; (52)).
383 Sustained clearance of calcium from the stereocilia bundle via PMCA2a pumps is

384 required to maintain calcium at physiological levels (53). Hair cells in the high frequency
385 region of the cochlea show larger amplitude current through mechanotransduction
386 channels corresponding with larger calcium influx. This generates a larger calcium load
387 entering the stereocilia of high frequency hair cells, resulting in greater levels of
388 metabolic stress on mitochondria (51). Therefore, the hair cell's ability to handle
389 intracellular calcium load may be predictive of hair cell susceptibility to environmental
390 and ototoxic stress. Our data shows increased vulnerability to cisplatin with cumulative
391 mitochondrial activity (Figure 2) as well as dysregulation of calcium homeostasis in all
392 hair cells exposed to cisplatin (Figure 3,4), possibly indicating that hair cells with greater
393 cumulative mitochondrial activity have a reduced capacity to regulate intracellular
394 calcium concentrations and are more susceptible to death from dysregulation driven by
395 cisplatin. This idea is further supported by the observation that hair cell mitochondrial
396 calcium measurements at baseline were not predictive of cisplatin vulnerability (i.e. that
397 mitochondria with less cumulative metabolic activity are better able to buffer intracellular
398 calcium levels even when stressed; Figure 6). Inhibiting mitochondrial calcium uptake
399 with either calcium chelators or pharmacological inhibitors has been shown to
400 significantly reduce neomycin induced hair cell death in lateral line neuromasts (27, 36).
401 Still to be determined is whether modulating mitochondrial calcium transients during a
402 critical window prior to the activation of Caspase-3 could provide protection from
403 cisplatin induced hair cell death. One important difference between neomycin-induced
404 and cisplatin-induced hair cell death in the zebrafish lateral line is that neomycin kills
405 hair cells within minutes, while cisplatin-induced death takes hours (32). A key
406 challenge to performing this experiment in cisplatin-treated zebrafish is determining

407 when and how to inhibit hair cell mitochondrial calcium uptake such that it provides
408 protection while minimally impacting normal hair cell respiration and metabolism (54).
409

410 ***Cisplatin accumulation in mitochondria correlates with hair cell death***

411 We observed mitochondrial accumulation of cisplatin in a subset of hair cells as an early
412 event predictive of hair cell death (Figure 6, 7), suggesting that this accumulation
413 triggers downstream cellular events that culminate in hair cell apoptosis. One likely
414 target for cisplatin in hair cells is mitochondrial DNA. Prior work has reported cisplatin-
415 induced mitochondrial DNA damage and mitochondrial degradation in dorsal root
416 ganglion neurons (55). Additional studies in head and neck cancer cell lines implicate
417 mitochondrial DNA as a major determinant of cisplatin sensitivity (56, 57). In addition,
418 mitochondrial membrane proteins, such as Voltage-dependent anion-selective channel
419 1 (VDAC-1), may also be directly targeted by cisplatin (56). Future work is needed to
420 identify mitochondrial target of cisplatin in sensory hair cells and to determine how
421 accumulation of cisplatin in mitochondria contributes to hair cell death.
422

423 ***Conclusion***

424 Cisplatin will continue to be a staple for solid and hematologic malignancies in the
425 coming decades. As such, developing strategies that ameliorate or prevent ototoxicity
426 should remain a focus of research and innovation. Using live *in vivo* imaging of
427 zebrafish lateral line organs, this study established that mitochondrial accumulation of
428 cisplatin precedes mitochondrial calcium dysregulation and eventual Caspase-3-
429 mediated hair cell death. Our findings advance the notion that mitochondria are key

430 mediators of cisplatin ototoxicity, and that they may even be direct targets of cisplatin
431 itself. Future investigations may seek to determine whether prevention of calcium
432 dysregulation reduces ototoxicity and to characterize the activity of cisplatin within
433 mitochondria. Such studies will provide further insight to the underpinnings of cisplatin
434 ototoxicity and guide additional targeted drug discovery.
435

436 **Methods:**

437 *Sex as a biological variable*

438 Sex cannot be determined or predicted in larval zebrafish. Larvae were therefore
439 chosen at random without consideration of sex.

440 *Zebrafish husbandry and lines*

441 Embryos were maintained in embryo media (EM: 15 mM NaCl, 0.5 mM KCl, 1 mM
442 $CaCl_2$, 1 mM $MgSO_4$, 0.015 mM KH_2PO_4, 0.042 mM Na_2HPO_4, 0.714 mM $NaHCO_3$) at
443 28°C with 14-hour light and 10-hour dark cycles (58). After 3 days post-fertilization (dpf),
444 larvae were transferred to 250-mL plastic beakers, raised in 100 – 200 mL of EM, and
445 fed rotifers daily. All experiments were performed on larvae aged 5 – 7 dpf

446 Previously described transgenic lines included: w119Tg (*Tg(myo6b:mitoGCaMP3)*;
447 (27)), w78Tg (*Tg(myo6b:cytoGCaMP3);* (36)), w208Tg (*Tg(myo6b:mitoTimer);* (21), and
448 y229Gt (*Tg(TNKS1bp1:EGFP);* (42). The first three lines were used to evaluate
449 changes in mitochondrial calcium levels, cytoplasmic calcium levels, and cumulative
450 mitochondrial activity, respectively. The last line expresses GFP in neuromast
451 supporting cells, permitting identification of hair cells in the absence of genetically

452 encoded biosensors. Fluorescent transgenic larvae were identified at 3 – 4 dpf under
453 anesthesia with 0.01% tricaine in EM.

454 *Zebrafish live imaging and cisplatin exposure protocol*

455 Larvae at 5 – 7 dpf were anesthetized in 0.01% tricaine methanesulfonate (MS-222) in
456 EM and mounted lateral-side up in an open bath image chamber (Warner Instruments;
457 RC-26G) with a coverglass bottom. A slice anchor (Warner Instruments; 64-0253) was
458 used to secure up to 3 larvae at a time. Larvae were maintained in approximately 1 mL
459 EM with 0.01% tricaine throughout the duration of the live imaging.

460 After larvae were immobilized, three baseline images were acquired in 5 min intervals.
461 Then, 4 – 5 volumes of EM containing 0.01% MS-222 (1 mL each) with or without
462 cisplatin (Abcam; ab141398) were exchanged around the mounted fish to initiate the
463 exposure protocol. After 2 hours of exposure, fish were rinsed with 4 – 5 volumes of EM
464 containing 0.01% MS-222 (1 mL each), maintained under sedation for an additional 2 –
465 4 hours depending on the specific experiment, and then euthanized.

466 For experiments with *mitoTimer* larvae, imaging was obtained before and after the
467 cisplatin exposure protocol. For time-lapse experiments, images were acquired every 10
468 minutes throughout the 4-hour exposure protocol.

469 *Experiments involving Rho-Mito*

470 Rho-Mito is a vital dye that localizes within mitochondria and fluoresces in the presence
471 of cisplatin (41). Larvae at 5 – 7 dpf expressing either GCaMP3 in mitochondria
472 (*Tg(myo6b:mitoGCaMP3))* or GFP in supporting cells (*Tg(TNKS1bp1:EGFP))* were
473 incubated in EM with or without 1 mM cisplatin for either 30 or 60 min, depending on the

474 experiment. This was followed by three rinses in EM. They were then submerged in EM
475 containing Rho-Mito 3 μM for 15 minutes. Next, the larvae were rinsed twice in EM and
476 then sedated and mounted for live imaging as previously described. Larvae expressing
477 *mitoGCaMP3* were imaged at baseline and after 4 additional hours of recovery in EM to
478 observe subsequent hair cell death. Larvae expressing GFP in supporting cells were
479 only imaged at their specified time point to evaluate the dynamics of cisplatin
480 accumulation within mitochondria.

481 *Image acquisition and analysis for live imaging*

482 Z-stack images (2 μm step size; 30 steps per Z-stack) of neuromasts L2 – L4 were
483 obtained with an ORCA-Flash 5.0 V3 camera (Hamamatsu) using an X-Light V2TP
484 spinning disk confocal and a 63x/0.9N.A. water immersion objective on a Leica DM6
485 Fixed Stage microscope. Green fluorescence from *mitoGCaMP3-, cytoGCaMP3-,* and
486 *mitoHyPer*-labeled hair cells and GFP-labeled supporting cells were imaged using a 470
487 nm wavelength laser at 20% power with a 50 ms/frame exposure time. Red
488 fluorescence from hair cells labeled with Rho-Mito were imaged using a 555 nm
489 wavelength laser at 20% power with a 50 ms/frame exposure time. In *mitoTimer*-labeled
490 hair cells, green and red fluorescence were measured simultaneously using a Cairn
491 OptoSplit II Bypass Image Splitter (Cairn Research Ltd). Multi-position image acquisition
492 was accomplished using a Motorized ZDeck Quick-Adjust Platform System (Prior
493 Scientific) directed by MetaMorph software (Molecular Devices).

494 Digital images of neuromasts were processed and analyzed using ImageJ software
495 (60). Evaluation of changes in fluorescent intensity of genetically encoded biosensors
496 was performed as previously described with a few modifications (59). In brief, maximum

497 intensity projections of each z-stack were generated, then background subtraction was
498 performed using a rolling ball radius of 100 pixels. A circular region of interest (ROI) with
499 a diameter of 4 μm was placed around each hair cell according to its baseline position.
500 Average fluorescence intensities within the ROI were then measured and expressed
501 relative to the median baseline intensity of control hair cells. For time-lapse
502 experiments, Stackreg and Turboreg ImageJ plugins were used for recursive alignment
503 of hair cells that drifted over the acquisition time (61). Hair cells were characterized as
504 living or dying based on their fragmentation and neuromast clearance (as described in
505 (36)). Data were excluded at time points when fragments of dying hair cells drifted into
506 neighboring ROIs of living hair cells.

507 *Microflume protocol*

508 Experiments with the microflume were adapted from methods that used an orbital
509 shaker to stimulate the lateral-line organ (21). Briefly, larvae at 5 dpf were transferred
510 into a microflume apparatus that produces a consistent flow stimulus of 5 mm/sec (~1
511 larval length/sec) (62). Larvae were exposed to this flow stimulus for 24 hours in EM.
512 Following exposure to microflume stimulation, larvae were immobilized and baseline
513 images were acquired. Then they were exposed to 250 μM cisplatin for 2 hours and
514 imaged after an additional 4 hours of recovery in EM with 0.01% tricaine. Imaging
515 processing and analysis were performed as in the other live imaging experiments with
516 the following modifications. Images were acquired with an exposure time of 100
517 ms/frame instead of 50 ms/frame. The ratio of *mitoTimer* red:green fluorescence for
518 each hair cell was calculated and normalized to the median value of control hair cells.

519 Hair cell counts per neuromast were expressed as a percentage of remaining intact hair
520 cells after cisplatin exposure compared to baseline.

521 *Whole-mount immunohistochemistry, imaging, and analysis of Caspase-3 experiments*

522 Cisplatin exposure and fixation with activated Caspase-3 antibodies were performed as
523 previously described with a few modifications (18). Briefly, groups of wildtype larvae
524 (AB*) at 6 dpf were incubated for 2 hours in 30 mL EM with or without 1 mM cisplatin
525 (Abcam) at 28˚C. Larvae were then rinsed and allowed to recover for an additional 2
526 hours in 30 mL EM. At every 30-minute increment starting immediately prior to
527 treatment initiation, groups of control and cisplatin-exposed larvae were euthanized by
528 rapid chilling and fixed overnight in 4% paraformaldehyde in 0.1 M phosphate-buffered
529 solution (PBS pH = 7.4) at 4˚C. The next day, fixed specimens were rinsed, blocked,
530 and incubated in primary antibodies (1:500 HCS-1 mouse monoclonal, DSHB,
531 University of Iowa; 1:400 anti-cleaved Caspase-3 rabbit polyclonal, Cell Signaling
532 Technology). After overnight incubation in primary, specimens were rinsed and
533 incubated in DAPI (5 µg/mL) and secondary antibodies (1:500 anti-mouse IgG
534 conjugated to Alexa Fluor 488 and 1:500 anti-rabbit IgG conjugated to Alexa Fluor 555)
535 at room temperature in darkness. Specimens were rinsed in PBS prior to being
536 mounted on glass slides with elvanol (13 % w/v polyvinyl alcohol, 33 % w/v glycerol, 1
537 % w/v DABCO (1,4 diazobicylo[2,2,2] octane) in 0.2 M Tris, pH 8.5).

538 The posterior lateral-line neuromasts (L3 – L5) of fixed and labeled zebrafish were
539 imaged as in the prior live imaging experiments, except that images were acquired with
540 an exposure time of 100 ms/frame and a step size of 1 µm. DAPI-stained hair cells were
541 acquired with a 405 nm wavelength laser. The percentage of hair cells with cleaved

542 Caspase-3 were determined for each neuromast and then averaged across neuromasts
543 present within the same fish to account for fish-to-fish variability.

544 *Statistics*

545 Standard descriptive statistics were used to describe experimental results. The
546 D'Agostino-Pearson test was used to determine normality of data. Differences between
547 two groups were determined using the unpaired Student's *t*-test or Mann-Whitney *U*
548 test, as appropriate. Comparison of multiple groups was performed by one-way ANOVA
549 or Kruskal-Wallis test depending on data normality with appropriate *post hoc* tests as
550 needed. A mixed model with Bonferroni *post hoc* analysis was performed on the
551 cleaved Caspase-3 experiments. All statistical analyses were conducted using Prism 9
552 (GraphPad Software Inc).

553 *Study approval*

554 All experiments on zebrafish were performed with the approval of the Institutional
555 Animal Care and Use Committee of Washington University School of Medicine in St.
556 Louis (Protocol number: 20-0158) and in accordance with NIH guidelines for
557 use of zebrafish.

558 *Data availability*

559 Underlying graphed data and reported means can be found in the Supporting Data
560 Values file. STL files of microflume components are available in the Open Science
561 Framework repository, https://osf.io/rvyfz/.

562 **Author contributions:**

563 DSL, WHA, MW, and LS contributed towards experimental design. DSL and AS
564 performed experiments, acquired data, and analyzed data. WHA and JZ additionally
565 provided reagents and guidance on experimental design. DSL, WHA, MW, and LS
566 contributed towards writing and revising the manuscript to its final form.

567

568 **Acknowledgements:**

569 Research reported in this publication was supported by a Large-Scale Interdisciplinary
570 Research Initiative from the Children's Discovery Institute, St. Louis Children's Hospital
571 (LS and MW; Grant # MC-LI-2018-762), the American Society of Pediatric
572 Otolaryngology CORE grant (DL.; # 930395), and the National Institute of Deafness and
573 Other Communication Disorders (NIDCD) within the National Institutes of Health (NIH),
574 through the "Development of Clinician/Researchers in Academic ENT" training grant,
575 award number T32DC000022 (DL). The content is solely the responsibility of the
576 authors and does not necessarily represent the official view of the funding sources. We
577 further acknowledge Emily L. Bell for her technical support in the live *in vivo* imaging
578 experiments.

579 **References**

580 1. Breglio AM, Rusheen AE, Shide ED, Fernandez KA, Spielbauer KK, McLachlin KM, et
581 al. Cisplatin is retained in the cochlea indefinitely following chemotherapy. *Nat Commun.*
582 2017;8(1):1654.
583 2. Frisina RD, Wheeler HE, Fossa SD, Kerns SL, Fung C, Sesso HD, et al. Comprehensive
584 Audiometric Analysis of Hearing Impairment and Tinnitus After Cisplatin-Based
585 Chemotherapy in Survivors of Adult-Onset Cancer. *J Clin Oncol.* 2016;34(23):2712-20.
586 3. Ardeshirrouhanifard S, Fossa SD, Huddart R, Monahan PO, Fung C, Song Y, et al.
587 Ototoxicity After Cisplatin-Based Chemotherapy: Factors Associated With Discrepancies
588 Between Patient-Reported Outcomes and Audiometric Assessments. *Ear Hear.*
589 2022;43(3):794-807.
590 4. Brock PR, Knight KR, Freyer DR, Campbell KC, Steyger PS, Blakley BW, et al.
591 Platinum-induced ototoxicity in children: a consensus review on mechanisms,
592 predisposition, and protection, including a new International Society of Pediatric
593 Oncology Boston ototoxicity scale. *J Clin Oncol.* 2012;30(19):2408-17.
594 5. Buchmann L, Conlee J, Hunt J, Agarwal J, and White S. Psychosocial distress is
595 prevalent in head and neck cancer patients. *Laryngoscope.* 2013;123(6):1424-9.
596 6. Ciorba A, Bianchini C, Pelucchi S, and Pastore A. The impact of hearing loss on the
597 quality of life of elderly adults. *Clin Interv Aging.* 2012;7:159-63.
598 7. Yu D, Gu J, Chen Y, Kang W, Wang X, and Wu H. Current Strategies to Combat
599 Cisplatin-Induced Ototoxicity. *Front Pharmacol.* 2020;11:999.
600 8. Chattaraj A, Syed MP, Low CA, and Owonikoko TK. Cisplatin-Induced Ototoxicity: A
601 Concise Review of the Burden, Prevention, and Interception Strategies. *JCO Oncol*
602 *Pract.* 2023:OP2200710.

603 9. Ciccarelli RB, Solomon MJ, Varshavsky A, and Lippard SJ. In vivo effects of cis- and
604 trans-diamminedichloroplatinum(II) on SV40 chromosomes: differential repair, DNA-
605 protein cross-linking, and inhibition of replication. *Biochemistry.* 1985;24(26):7533-40.
606 10. Ormerod MG, Orr RM, and Peacock JH. The role of apoptosis in cell killing by cisplatin:
607 a flow cytometric study. *Br J Cancer.* 1994;69(1):93-100.
608 11. Pinto AL, and Lippard SJ. Sequence-dependent termination of in vitro DNA synthesis by
609 cis- and trans-diamminedichloroplatinum (II). *Proc Natl Acad Sci U S A.*
610 1985;82(14):4616-9.
611 12. Sheth S, Mukherjea D, Rybak LP, and Ramkumar V. Mechanisms of Cisplatin-Induced
612 Ototoxicity and Otoprotection. *Front Cell Neurosci.* 2017;11:338.
613 13. Kros CJ, and Steyger PS. Aminoglycoside- and Cisplatin-Induced Ototoxicity:
614 Mechanisms and Otoprotective Strategies. *Cold Spring Harb Perspect Med.* 2019;9(11).
615 14. Boveris A, and Chance B. The mitochondrial generation of hydrogen peroxide. General
616 properties and effect of hyperbaric oxygen. *Biochemical Journal.* 1973;134(3):707-16.
617 15. Balaban RS, Nemoto S, and Finkel T. Mitochondria, oxidants, and aging. *cell.*
618 2005;120(4):483-95.
619 16. Borse V, Al Aameri RFH, Sheehan K, Sheth S, Kaur T, Mukherjea D, et al.
620 Epigallocatechin-3-gallate, a prototypic chemopreventative agent for protection against
621 cisplatin-based ototoxicity. *Cell Death Dis.* 2017;8(7):e2921.
622 17. Alam SA, Ikeda K, Oshima T, Suzuki M, Kawase T, Kikuchi T, et al. Cisplatin-induced
623 apoptotic cell death in Mongolian gerbil cochlea. *Hear Res.* 2000;141(1-2):28-38.
624 18. Lee DS, Schrader A, Warchol M, and Sheets L. Cisplatin exposure acutely disrupts
625 mitochondrial bioenergetics in the zebrafish lateral-line organ. *Hear Res.*
626 2022;426:108513.

627 19. Li H, Helpard L, Ekeroot J, Rohani SA, Zhu N, Rask-Andersen H, et al. Three-
628 dimensional tonotopic mapping of the human cochlea based on synchrotron radiation
629 phase-contrast imaging. *Sci Rep.* 2021;11(1):4437.
630 20. Prayuenyong P, Baguley DM, Kros CJ, and Steyger PS. Preferential Cochleotoxicity of
631 Cisplatin. *Front Neurosci.* 2021;15:695268.
632 21. Pickett SB, Thomas ED, Sebe JY, Linbo T, Esterberg R, Hailey DW, et al. Cumulative
633 mitochondrial activity correlates with ototoxin susceptibility in zebrafish mechanosensory
634 hair cells. *Elife.* 2018;7.
635 22. Engel J, Braig C, Rüttiger L, Kuhn S, Zimmermann U, Blin N, et al. Two classes of outer
636 hair cells along the tonotopic axis of the cochlea. *Neuroscience.* 2006;143(3):837-49.
637 23. Sha S-H, Taylor R, Forge A, and Schacht J. Differential vulnerability of basal and apical
638 hair cells is based on intrinsic susceptibility to free radicals. *Hearing research.*
639 2001;155(1-2):1-8.
640 24. Esterberg R, Linbo T, Pickett SB, Wu P, Ou HC, Rubel EW, et al. Mitochondrial calcium
641 uptake underlies ROS generation during aminoglycoside-induced hair cell death. *J Clin*
642 *Invest.* 2016;126(9):3556-66.
643 25. Fujimoto C, and Yamasoba T. Oxidative stresses and mitochondrial dysfunction in age-
644 related hearing loss. *Oxid Med Cell Longev.* 2014;2014:582849.
645 26. Zou T, Ye B, Chen K, Zhang A, Guo D, Pan Y, et al. Impacts of impaired mitochondrial
646 dynamics in hearing loss: Potential therapeutic targets. *Front Neurosci.* 2022;16:998507.
647 27. Esterberg R, Hailey DW, Rubel EW, and Raible DW. ER-mitochondrial calcium flow
648 underlies vulnerability of mechanosensory hair cells to damage. *J Neurosci.*
649 2014;34(29):9703-19.
650 28. Holmgren M, and Sheets L. Using the Zebrafish Lateral Line to Understand the Roles of
651 Mitochondria in Sensorineural Hearing Loss. *Front Cell Dev Biol.* 2020;8:628712.

652 29. Coffin A, Kelley M, Manley GA, and Popper AN. In: Manley GA, Fay RR, and Popper AN
653 eds. *Evolution of the Vertebrate Auditory System*. New York, NY: Springer New York;
654 2004:55-94.
655 30. Domarecka E, Skarzynska M, Szczepek AJ, and Hatzopoulos S. Use of zebrafish larvae
656 lateral line to study protection against cisplatin-induced ototoxicity: A scoping review. *Int*
657 *J Immunopathol Pharmacol.* 2020;34:2058738420959554.
658 31. Wertman JN, Melong N, Stoyek MR, Piccolo O, Langley S, Orr B, et al. The identification
659 of dual protective agents against cisplatin-induced oto- and nephrotoxicity using the
660 zebrafish model. *Elife.* 2020;9.
661 32. Lee DS, Schrader A, Bell E, Warchol ME, and Sheets L. Evaluation of Cisplatin-Induced
662 Pathology in the Larval Zebrafish Lateral Line. *Int J Mol Sci.* 2022;23(22).
663 33. Thomas AJ, Hailey DW, Stawicki TM, Wu P, Coffin AB, Rubel EW, et al. Functional
664 mechanotransduction is required for cisplatin-induced hair cell death in the zebrafish
665 lateral line. *J Neurosci.* 2013;33(10):4405-14.
666 34. Terskikh A, Fradkov A, Ermakova G, Zaraisky A, Tan P, Kajava AV, et al. "Fluorescent
667 timer": protein that changes color with time. *Science.* 2000;290(5496):1585-8.
668 35. Verkhusha VV, Chudakov DM, Gurskaya NG, Lukyanov S, and Lukyanov KA. Common
669 pathway for the red chromophore formation in fluorescent proteins and chromoproteins.
670 *Chem Biol.* 2004;11(6):845-54.
671 36. Esterberg R, Hailey DW, Coffin AB, Raible DW, and Rubel EW. Disruption of
672 intracellular calcium regulation is integral to aminoglycoside-induced hair cell death. *J*
673 *Neurosci.* 2013;33(17):7513-25.
674 37. Kleih M, Bopple K, Dong M, Gaissler A, Heine S, Olayioye MA, et al. Direct impact of
675 cisplatin on mitochondria induces ROS production that dictates cell fate of ovarian
676 cancer cells. *Cell Death Dis.* 2019;10(11):851.

677 38. Marullo R, Werner E, Degtyareva N, Moore B, Altavilla G, Ramalingam SS, et al.
678 Cisplatin induces a mitochondrial-ROS response that contributes to cytotoxicity
679 depending on mitochondrial redox status and bioenergetic functions. *PLoS One.*
680 2013;8(11):e81162.
681 39. Rizzuto R, De Stefani D, Raffaello A, and Mammucari C. Mitochondria as sensors and
682 regulators of calcium signalling. *Nat Rev Mol Cell Biol.* 2012;13(9):566-78.
683 40. Kiss RC, Xia F, and Acklin S. Targeting DNA Damage Response and Repair to Enhance
684 Therapeutic Index in Cisplatin-Based Cancer Treatment. *Int J Mol Sci.* 2021;22(15).
685 41. Ong JX, Le HV, Lee VEY, and Ang WH. A Cisplatin-Selective Fluorescent Probe for
686 Real-Time Monitoring of Mitochondrial Platinum Accumulation in Living Cells. *Angew*
687 *Chem Int Ed Engl.* 2021;60(17):9264-9.
688 42. Behra M, Gallardo VE, Bradsher J, Torrado A, Elkahloun A, Idol J, et al. Transcriptional
689 signature of accessory cells in the lateral line, using the Tnk1bp1:EGFP transgenic
690 zebrafish line. *BMC Developmental Biology.* 2012;12(1):6.
691 43. Saettele AL, Wong HC, Kindt KS, Warchol ME, and Sheets L. Prolonged
692 Dexamethasone Exposure Enhances Zebrafish Lateral-Line Regeneration But Disrupts
693 Mitochondrial Homeostasis and Hair Cell Function. *J Assoc Res Otolaryngol.*
694 2022;23(6):683-700.
695 44. Lukasz D, Beirl A, and Kindt K. Chronic neurotransmission increases the susceptibility of
696 lateral-line hair cells to ototoxic insults. *Elife.* 2022;11.
697 45. Chattaraj A, Syed MP, Low CA, and Owonikoko TK. Cisplatin-Induced Ototoxicity: A
698 Concise Review of the Burden, Prevention, and Interception Strategies. *JCO Oncol*
699 *Pract.* 2023;19(5):278-83.
700 46. Hellberg V, Wallin I, Ehrsson H, and Laurell G. Cochlear pharmacokinetics of cisplatin:
701 an in vivo study in the guinea pig. *Laryngoscope.* 2013;123(12):3172-7.

702 47. Sha SH, Taylor R, Forge A, and Schacht J. Differential vulnerability of basal and apical
703 hair cells is based on intrinsic susceptibility to free radicals. *Hear Res.* 2001;155(1-2):1-
704 8.
705 48. Jensen-Smith HC, Hallworth R, and Nichols MG. Gentamicin rapidly inhibits
706 mitochondrial metabolism in high-frequency cochlear outer hair cells. *PLoS One.*
707 2012;7(6):e38471.
708 49. Chen Y, Li L, Ni W, Zhang Y, Sun S, Miao D, et al. Bmi1 regulates auditory hair cell
709 survival by maintaining redox balance. *Cell Death Dis.* 2015;6(1):e1605.
710 50. Banerjee Mustafi S, Aznar N, Dwivedi SK, Chakraborty PK, Basak R, Mukherjee P, et al.
711 Mitochondrial BMI1 maintains bioenergetic homeostasis in cells. *FASEB J.*
712 2016;30(12):4042-55.
713 51. Fettiplace R, and Nam JH. Tonotopy in calcium homeostasis and vulnerability of
714 cochlear hair cells. *Hear Res.* 2019;376:11-21.
715 52. O'Sullivan JDB, Bullen A, and Mann ZF. Mitochondrial form and function in hair cells.
716 *Hear Res.* 2023;428:108660.
717 53. Dumont RA, Lins U, Filoteo AG, Penniston JT, Kachar B, and Gillespie PG. Plasma
718 membrane Ca2+-ATPase isoform 2a is the PMCA of hair bundles. *J Neurosci.*
719 2001;21(14):5066-78.
720 54. Llorente-Folch I, Rueda CB, Pardo B, Szabadkai G, Duchen MR, and Satrustegui J. The
721 regulation of neuronal mitochondrial metabolism by calcium. *J Physiol.*
722 2015;593(16):3447-62.
723 55. Podratz JL, Knight AM, Ta LE, Staff NP, Gass JM, Genelin K, et al. Cisplatin induced
724 mitochondrial DNA damage in dorsal root ganglion neurons. *Neurobiol Dis.*
725 2011;41(3):661-8.
726 56. Yang Z, Schumaker LM, Egorin MJ, Zuhowski EG, Guo Z, and Cullen KJ. Cisplatin
727 preferentially binds mitochondrial DNA and voltage-dependent anion channel protein in

728 the mitochondrial membrane of head and neck squamous cell carcinoma: possible role
729 in apoptosis. *Clin Cancer Res.* 2006;12(19):5817-25.
730 57. Aminuddin A, Ng PY, Leong CO, and Chua EW. Mitochondrial DNA alterations may
731 influence the cisplatin responsiveness of oral squamous cell carcinoma. *Sci Rep.*
732 2020;10(1):7885.
733 58. Westerfield M. *The Zebrafish Book. A Guide for the Laboratory Use of Zebrafish (Danio*
734 *rerio).* Eugene: University of Oregon Press; 2000.
735 59. Lukasz D, and Kindt KS. In Vivo Calcium Imaging of Lateral-line Hair Cells in Larval
736 Zebrafish. *J Vis Exp.* 2018(141).
737 60. Schneider CA, Rasband WS, and Eliceiri KW. NIH Image to ImageJ: 25 years of image
738 analysis. *Nat Methods.* 2012;9(7):671-5.
739 61. Thevenaz P, Ruttimann UE, and Unser M. A pyramid approach to subpixel registration
740 based on intensity. *IEEE transactions on image processing.* 1998;7(1):27-41.
741 62. Newton KC, Kacev D, Nilsson SRO, Saettele AL, Golden SA, and Sheets L. Lateral line
742 ablation by ototoxic compounds results in distinct rheotaxis profiles in larval zebrafish.
743 *Commun Biol.* 2023;6(1):84.

744

745

746 **Figures**

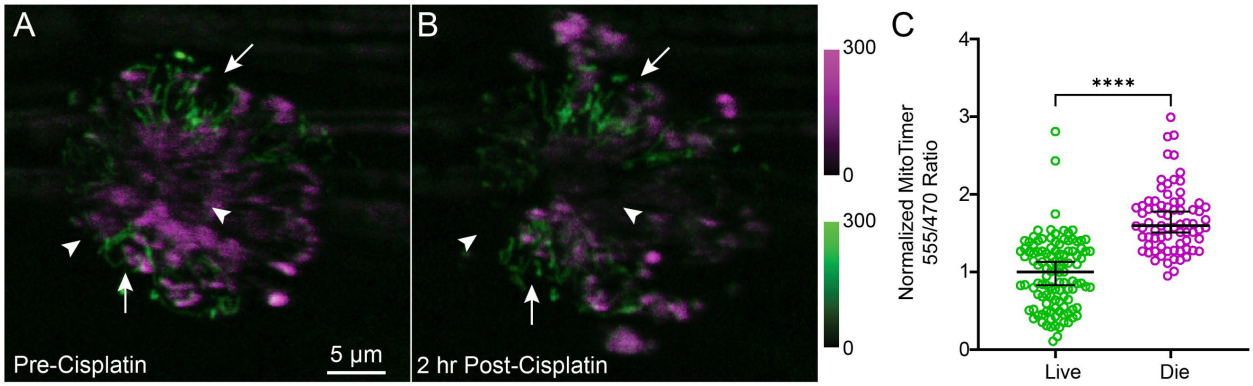

747
748 **Figure 1. Cumulative mitochondrial activity increases hair cell susceptibility to cisplatin. (A –**
749 **B)** Maximum-intensity projections of confocal z-stack images of *Tg(myo6b:mitoTimer)* neuromasts
750 prior to (**A**) and after (**B**) 2 h cisplatin (1 mM) exposure followed by 2 h recovery in EM.
751 Representative hair cells with high baseline cumulative mitochondrial activity (high 555/470 ratio) are
752 indicated by arrowheads and representative hair cells with low cumulative mitochondrial activity (low
753 555/470 ratio) are indicated by arrows. **(C)** Baseline ratios of mitoTimer fluorescence (normalized to
754 median of control) indicate that dying hair cells exhibit significantly higher ratios red to green ratios
755 than surviving hair cells (Mann-Whitney U test, ****$p < 0.0001$). Median values with corresponding
756 95% confidence intervals shown. n = 113 alive hair cells, 75 dead hair cells; N = 3 trials, 2 zebrafish
757 per trial, 3 neuromasts per zebrafish.
758

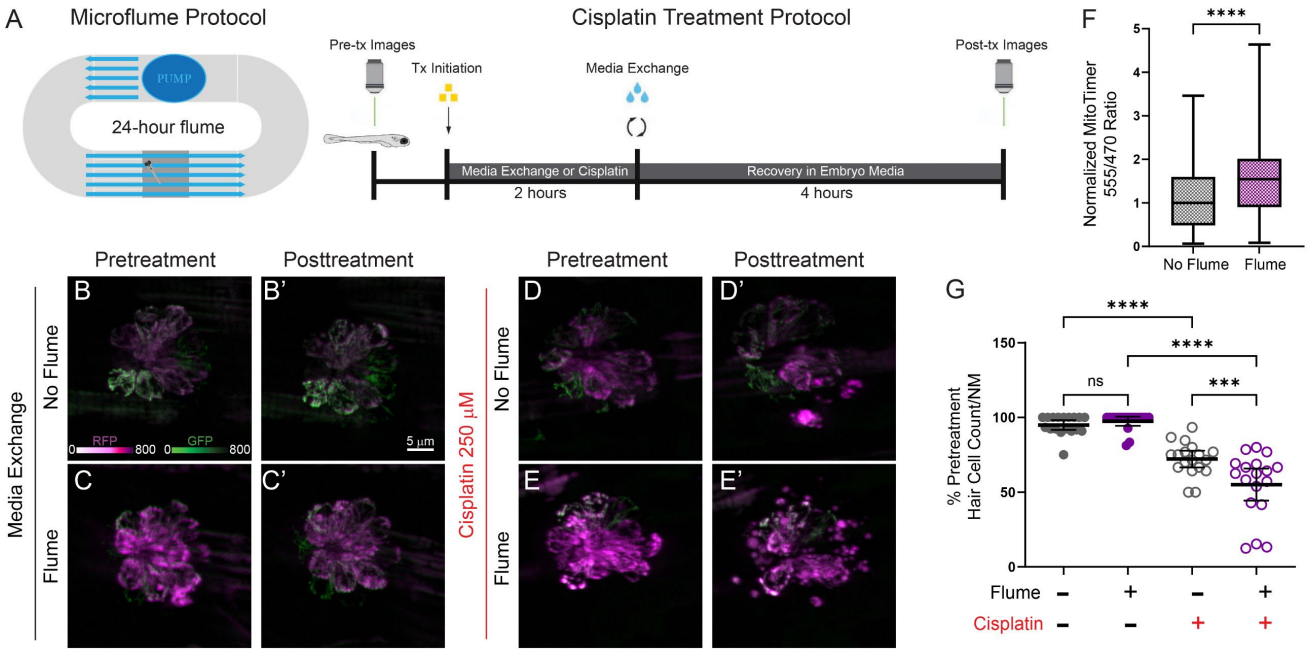

Figure 2. Sustained lateral line hair cell stimulation increases cumulative mitochondrial activity and susceptibility to cisplatin. (A) Schematic of the microflume and workflow of the cisplatin treatment protocol. **(B – E)** Maximum-intensity projections of confocal z-stack images of *Tg(myo6b:mitoTimer)* zebrafish neuromasts prior to (**B, C, D, E**) and after 2 h treatment with either EM (media exchange; **B', C'**) or 250 µM cisplatin (**D', E'**) followed by recovery in EM for 2 h. Prior to initiating the exposure protocol, zebrafish either underwent incubation with no water flow for 24 h (**B**, **D**) or sustained stimulation to water flow in a flume for 24 h (**C**, **E**). **(F)** Ratios of mitoTimer fluorescence (normalized to no flume condition) after completion of a 24 h incubation in the presence or absence of sustained water flow indicate that prolonged hair cell stimulation increases cumulative mitochondrial activity (Mann-Whitney U test, ****$p < 0.0001$). **(G)** Percent of baseline hair cells per neuromast after completion of the cisplatin treatment protocol indicate that moderate-dose cisplatin (250 µM) kills a greater proportion of hair cells among flume stimulated versus unstimulated lateral line neuromasts (Tukey's multiple comparisons test, adjusted ns = 0.94, ****, $p < 0.0001$; **p = 0.0012). Median and mean values with corresponding 95% confidence intervals shown for (**F**) and (**G**), respectively. n = 458 hair cells no flume, 466 hair cells in flume; N = 3 trials, 6 zebrafish per condition per trial, 2 – 3 neuromasts per zebrafish.

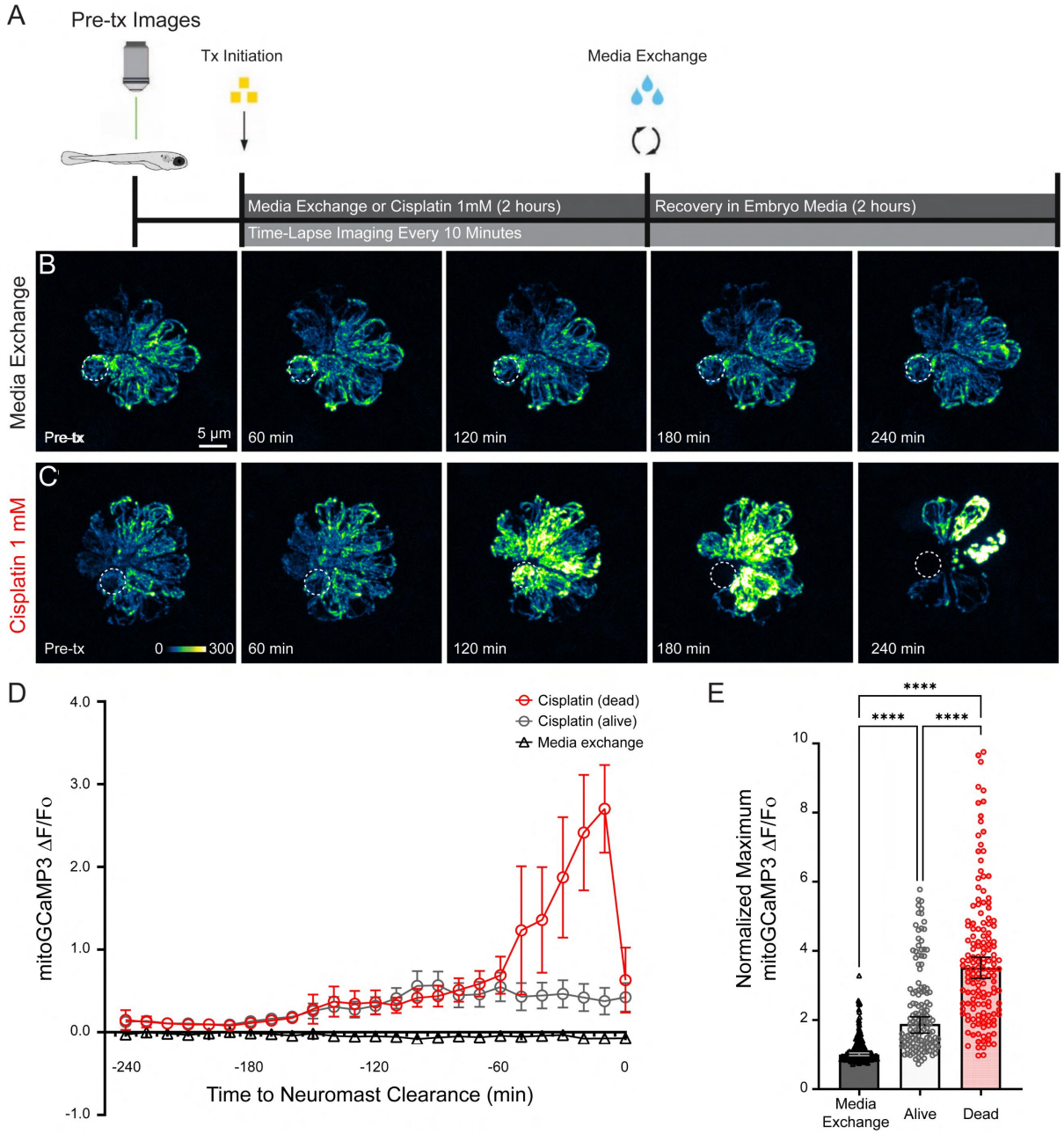

Figure 3. Elevated mitochondrial Ca^{2+} uptake is observed in all cisplatin exposed hair cells and progressively increases prior to hair cell death. (A) Schematic of cisplatin exposure and *in vivo* live imaging workflow. **(B – C)** Maximum-intensity projections of time-lapse confocal z-stack images show *Tg(myo6b:mitoGCaMP3)* zebrafish neuromasts at various points throughout the exposure protocol. Zebrafish were treated with either 2 h of EM (media exchange; **B**) or 1 mM cisplatin (**C**) followed by 2 h recovery in embryo media. Dotted circles indicate a representative 4 µm region of interest (ROI) in an individual hair cell used to measure mean mitoGCaMP3 fluorescence intensity. An ROI was applied to every hair cell within each neuromast. **(D)** Changes in mitoGCaMP3 fluorescence intensity relative to mean baseline fluorescence intensity ($\Delta F/F_O$) for each neuromast hair cell over time. Hair cells were grouped by treatment. Cisplatin-exposed hair cells were further categorized into those alive or dead at the conclusion of the exposure protocol. Data are aligned

792 relative to when dying hair cells were cleared from the neuromast. **(E)** Maximum change in
793 fluorescence relative to baseline (normalized to control) demonstrates significant differences in
794 mitochondrial Ca^{2+} levels between all three groups of hair cells (Dunn's multiple comparisons test,
795 ****adjusted $p < 0.0001$). Median values with corresponding 95% confidence intervals shown for
796 both (**C**) and (**D**). n = 233 media exchange hair cells, 136 alive cisplatin-exposed hair cells, 155 dead
797 cisplatin-exposed hair cells; N = 3 trials, 3 zebrafish per trial, 2 – 3 neuromasts per zebrafish.
798
799 **Movie 1.** The corresponding time lapse video of Figure 3C showing changes in hair cell
800 mitochondrial Ca^{2+} during and after cisplatin exposure.
801

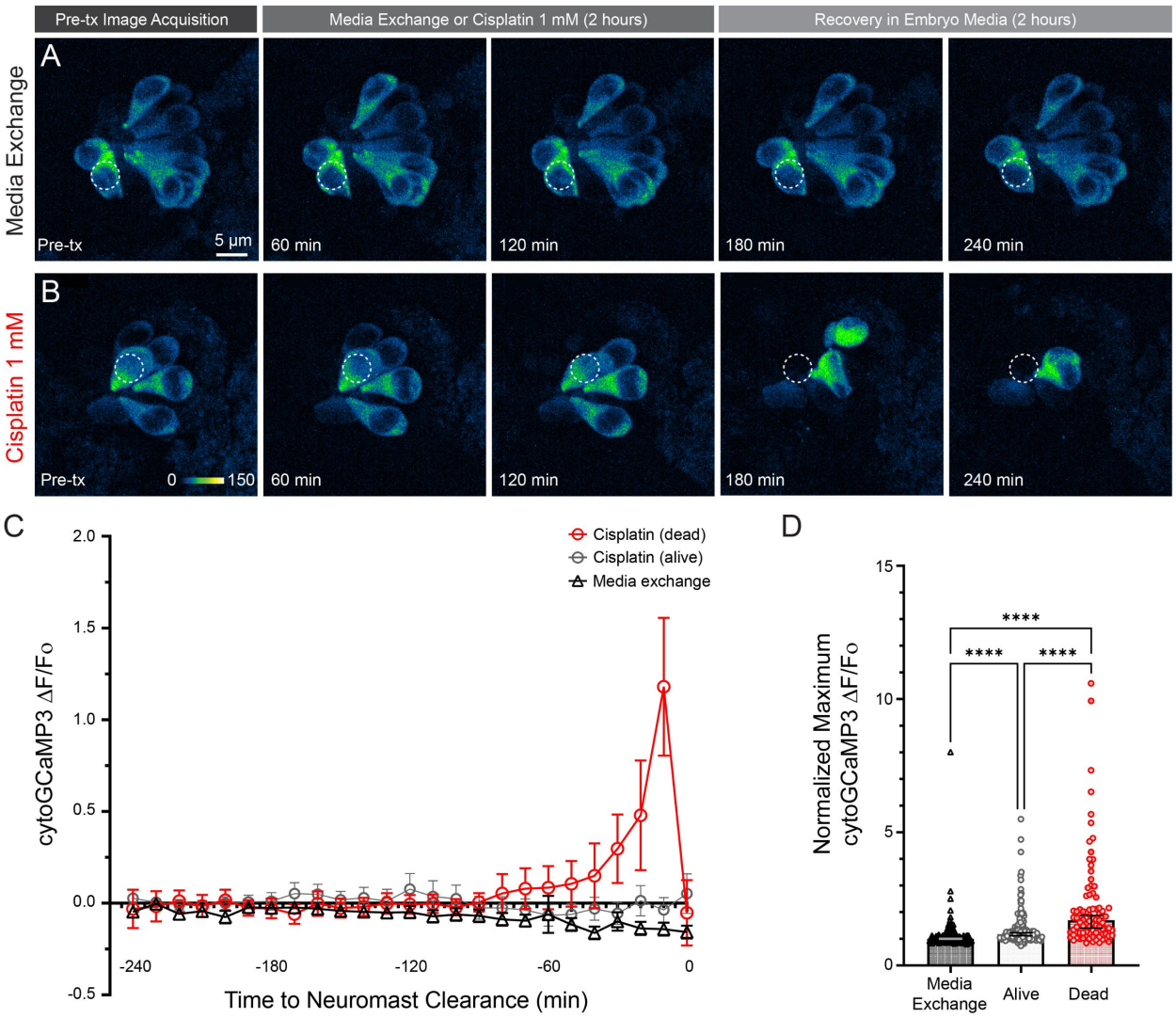

Figure 4. Elevated cytosolic Ca^{2+} uptake precedes cisplatin-induced hair cell death. (A – B) Maximum-intensity projections of time-lapsed confocal z-stack images show *Tg(myo6b:cytoGCaMP3)* zebrafish neuromasts at various points throughout the exposure protocol. Zebrafish were treated with either 2 h of EM (media exchange; **A**) or 1 mM cisplatin (**B**) followed by 2 h recovery in EM. Dotted circles indicate representative 4 µm ROI used to measure mean mitoGCaMP3 fluorescence intensity. **(C)** Changes in cytoGCaMP3 fluorescence intensity relative to baseline ($\Delta F/F_O$) for each hair cell over time. Data are aligned relative to when dying hair cells were cleared from the neuromast. **(D)** Comparison of maximum change in fluorescence relative to baseline (normalized to media exchange) demonstrates significant differences in cytosolic Ca^{2+} accumulation between all three groups of hair cells (Dunn's multiple comparisons test, ****adjusted $p < 0.0001$). Median values with corresponding 95% confidence intervals shown for both (**C**) and (**D**). n = 169 media exchange hair cells, 155 alive cisplatin-exposed hair cells, 87 dead cisplatin-exposed hair cells; N = 2 trials for media exchange and 4 trials for cisplatin 1 mM, 3 zebrafish per trial, 2 – 3 neuromasts per zebrafish.

Movie 2. The corresponding time lapse video of Figure 4B showing changes in hair cell cytosolic Ca2+ during and after cisplatin exposure.

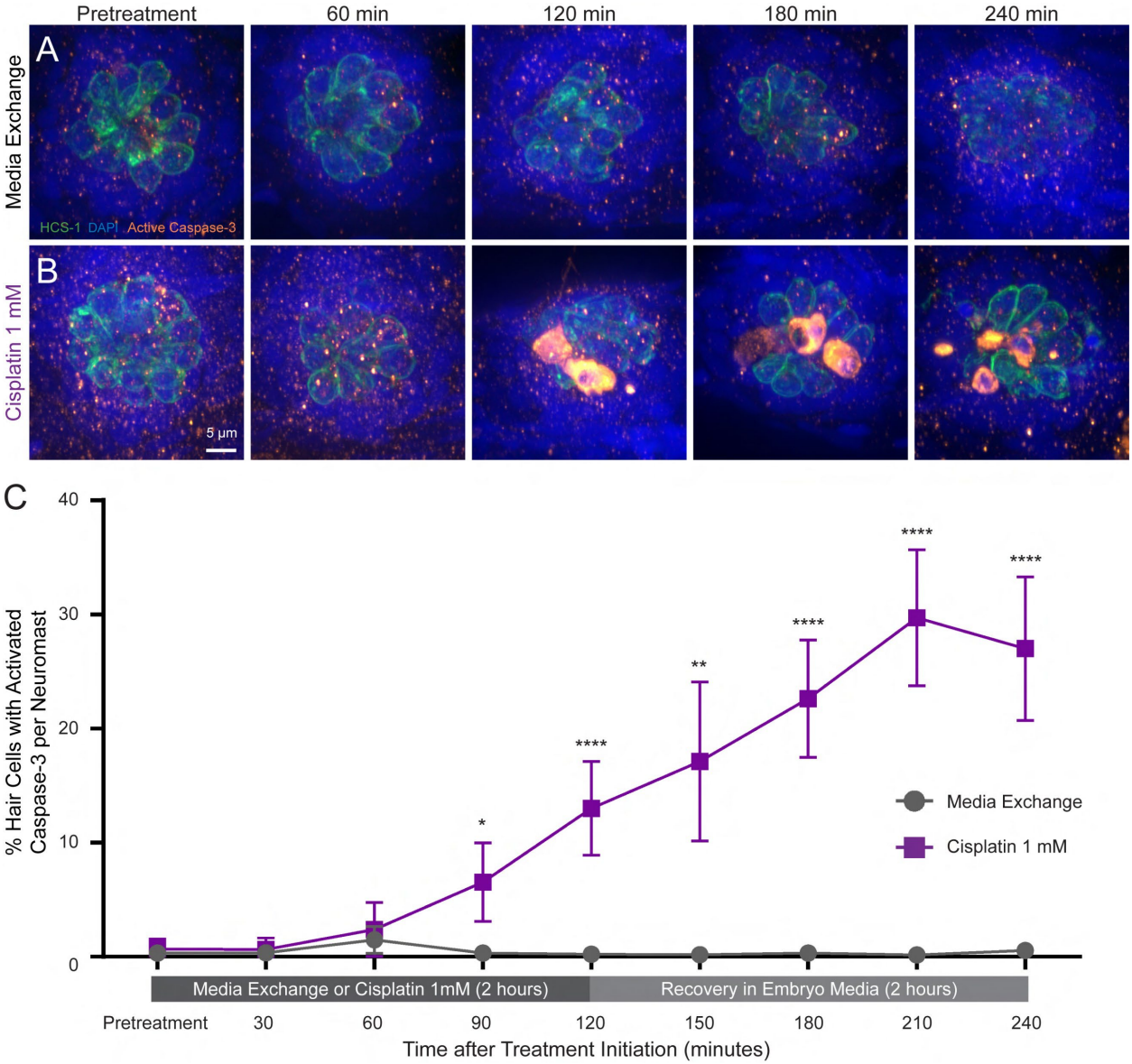

Figure 5. Progressive activation of Caspase-3 in a subset of neuromast hair cells initiates within 90 minutes of 1 mM cisplatin exposure. (A – B) Maximum-intensity projections of z-stack confocal images of immunolabled neuromasts at various points throughout the cisplatin exposure protocol. Zebrafish were treated for various amounts of time with either media exchange (**A**) or 1 mM cisplatin (**B**) followed by recovery in embryo media for up to 2 h. Hair cells were identified by immunolabel of Otoferlin (Hair Cell Soma-1; green) and stained for cleaved Caspase-3 (orange). All cell nuclei were labeled with DAPI (blue). **(C)** Percentage of hair cells per neuromast with activated Caspase-3 throughout the cisplatin exposure protocol. Neuromasts of cisplatin-treated zebrafish demonstrate a significantly greater proportion of hair cells with cleaved Caspase-3 starting at 90 minutes following exposure to cisplatin (Bonferroni's multiple comparisons test, **adjusted $p = 0.016$, ***adjusted $p = 0.0012$, ****adjusted $p < 0.0001$; Table 2). Mean values with corresponding 95% confidence intervals shown. n = 42 – 45 neuromasts per group; N = 3 trials, 4 – 5 zebrafish per trial, 2 – 3 neuromasts per zebrafish.

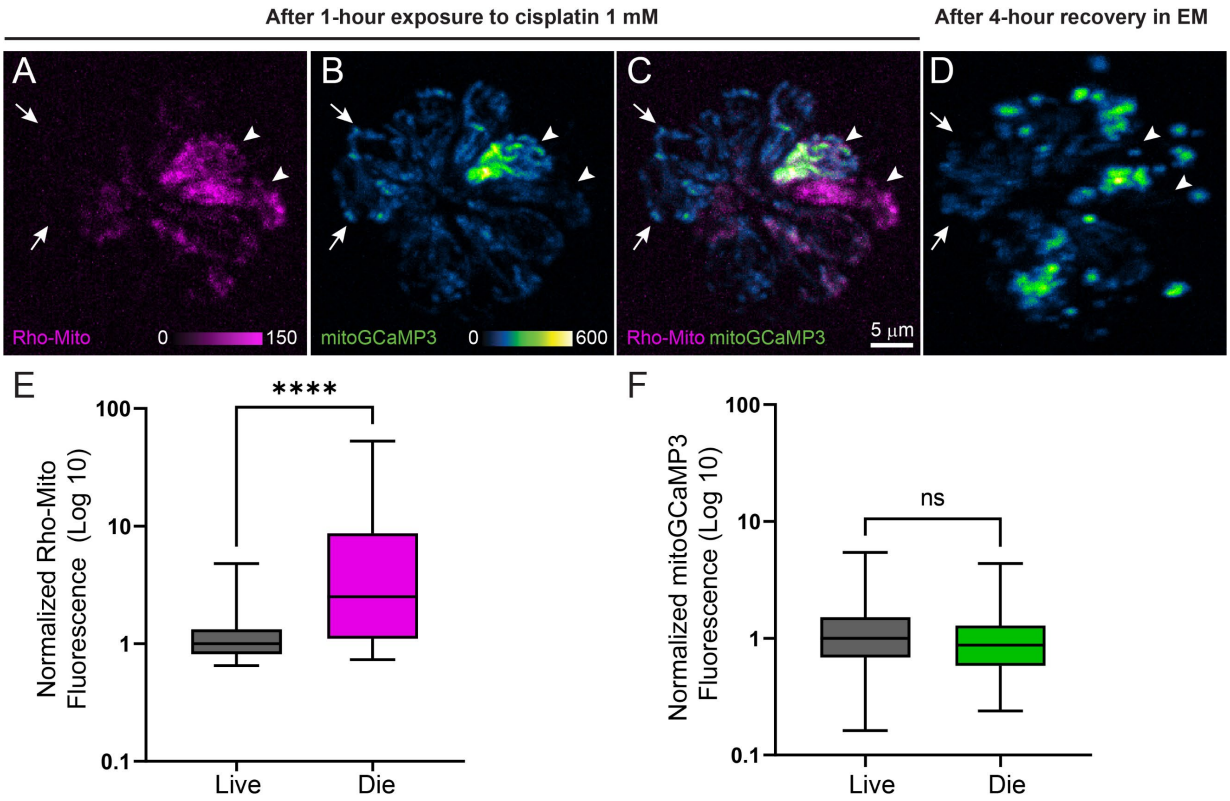

Figure 6. Mitochondrial accumulation of cisplatin corresponds with hair cell death. (A – D) Maximum-intensity projections of the same *Tg(myo6b:mitoGCaMP3]* neuromast after exposure to 1mM cisplatin for 1 h (**A – C**) followed by an additional 4 h recovery in EM (**D**). Rho-Mito fluorescence is observed within some, but not all, hair cell mitochondria. Hair cells with elevated Rho-Mito fluorescence following incubation in cisplatin are indicated by arrowheads and hair cells with minimal Rho-Mito fluorescence are indicated by arrows. **(E)** Dying hair cells exhibit significantly more Rho-Mito fluorescence than living hair cells (Mann-Whitney U test, ****$p < 0.0001$). (F) MitoGCaMP3 fluorescence in dying hair cells is not significantly different than living hair cells immediately following 1 h cisplatin exposure (Mann-Whitney U test, ns = 0.14). Median values with corresponding 95% confidence intervals shown. n = 229 alive hair cells, 92 dead hair cells; N = 3 trials, 2 – 3 zebrafish per trial, 2 – 3 neuromasts per zebrafish.

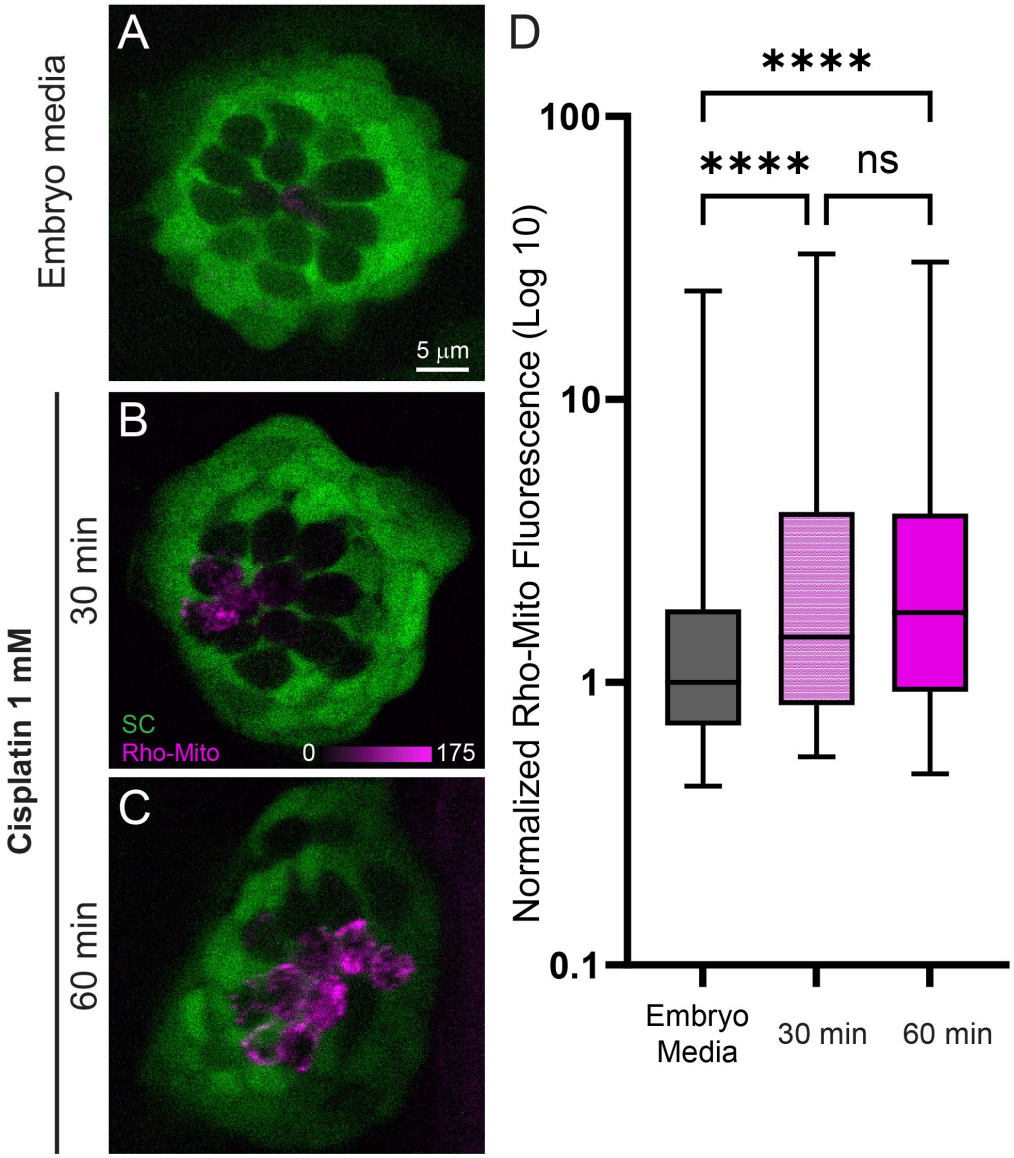

Figure 7. Cisplatin accumulates within hair cell mitochondria shortly after exposure. (A – C) Maximum-intensity projections of confocal z-stack images show (*Tg(TNKS1bp1:EGFP)* larvae expressing GFP in neuromast supporting cells at various time points after exposure to cisplatin. Zebrafish were treated with either EM (**A**) or 1 mM cisplatin for up to 1 h (**B** – **C**) followed by a 15 min incubation in 3 µM Rho-Mito. Hair cells were identified as GFP-negative silhouettes. **(D)** Relative fluorescence of Rho-Mito in hair cells normalized to the median of the control. Hair cells exposed to cisplatin demonstrate a significantly greater amount of Rho-Mito fluorescence at all time points (Dunn's multiple comparisons test, ****adjusted $p < 0.0001$). Although cisplatin appears to progressively accumulate in mitochondria over time, this trend was not significant (Dunn's multiple comparisons test, adjusted ns > 0.9999). Median values with corresponding 95% confidence intervals shown. n = 287 media exchange hair cells, 337 hair cells after 30 min cisplatin, 320 hair cells after 60 min cisplatin; N = 3 trials for control and cisplatin-exposed groups, 2 – 3 zebrafish per trial, 2 – 3 neuromasts per zebrafish.

867 **Tables**

868

869 **Table 1.** Time to half maximum ΔF/Fo prior to clearance from neuromast and after
870 exposure to cisplatin.

871

	Biosensor	Mean (min.)	95% confidence interval (min.)	Comparison	Mean difference (min.)	95% confidence interval (min.)	Adjusted *p* value
$t_{1/2}$ max ΔF/Fo prior to NM clearance	mitoGCaMP3	-36.3	-39.6 to -32.9	cytoGCaMP3	-11.3	-16.7 to -5.9	<0.0001
	cytoGCaMP3	-24.9	-27.4 to -22.5	mitoGCaMP3	11.3	5.9 to 16.7	<0.0001
$t_{1/2}$ max ΔF/Fo after cisplatin	mitoGCaMP3	131.8	123.9 to 139.7	cytoGCaMP3	19.7	5.3 to 34.2	0.0041
	cytoGCaMP3	112.1	100.9 to 123.2	mitoGCaMP3	-19.7	-34.2 to -5.3	0.0041

872

873 Mean data from individual hair cells shown in Figures 3 and 4. (NM = neuromast)

874

875 **Table 2.** Results from repeated measures mixed model of Caspase-3 activation in the
876 presence or absence of cisplatin 1 mM.

877

Time after assay initiation (min.)	Exposure group (% HC with activated Caspase-3/NM)		Mean difference (%)	95% confidence interval (%)	Adjusted *p* value
	Cisplatin 1 mM	Media exchange			
0	0.67	0.33	0.34	-1.1 to 1.8	>0.9999
30	0.63	0.34	0.29	-1.3 to 1.9	>0.9999
60	2.4	1.48	0.9082	-2.9 to 4.7	>0.9999
90	6.55	0.33	6.22	0.92 to 11.5	0.016
120	13.0	0.22	12.78	6.5 to 19.1	<0.001
150	17.1	0.17	16.9	6.3 to 27.6	0.0012
180	22.6	0.32	22.3	14.4 to 30.2	<0.001
210	29.7	0.16	29.5	20.5 to 38.6	<0.001
240	27.0	0.56	26.5	16.8 to 36.1	<0.001

878

879 Mean percentages of hair cells with activated-Caspase 3 from neuromasts shown in
880 Figure 5. (HC = hair cell, NM = neuromast)

Figure 1

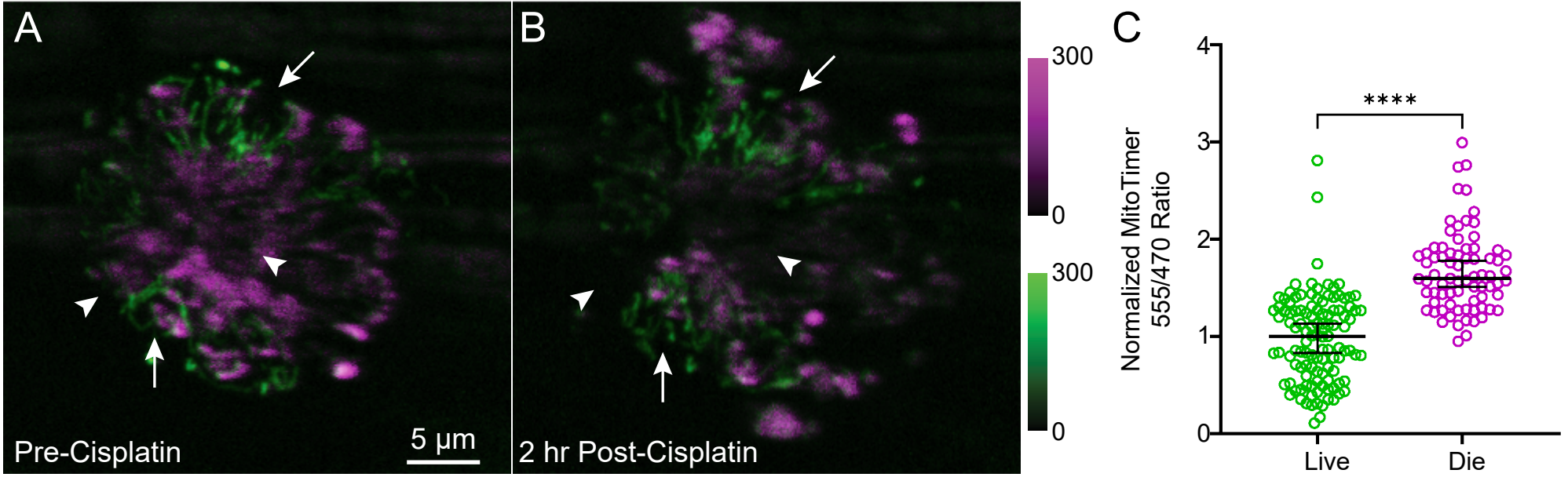
A
B
C
Pre-Cisplatin
5 µm
2 hr Post-Cisplatin
300
0
300
0
Normalized MitoTimer
555/470 Ratio
4
3
2
1
0
****
Live
Die

Figure 2

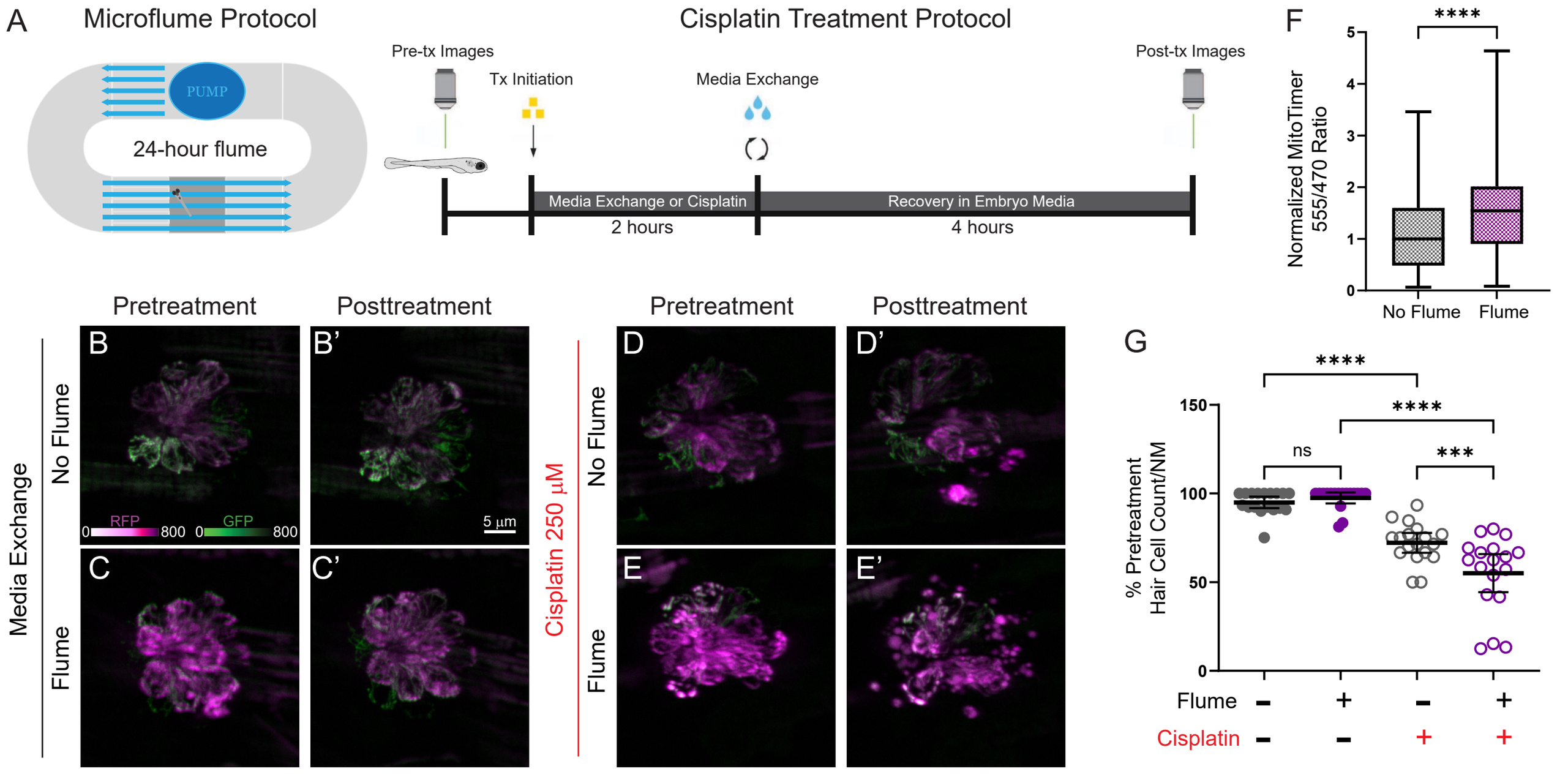
A
Microflume Protocol
PUMP
24-hour flume
Cisplatin Treatment Protocol
Pre-tx Images
Tx Initiation
Media Exchange
Post-tx Images
Media Exchange or Cisplatin
2 hours
Recovery in Embryo Media
4 hours
F
Normalized MitoTimer 555/470 Ratio
****
No Flume
Flume
Pretreatment
Posttreatment
Media Exchange
No Flume
Flume
B
B'
C
C'
RFP
GFP
0
800
5 µm
Cisplatin 250 µM
D
D'
E
E'
G
% Pretreatment Hair Cell Count/NM
****
****
ns
***
Flume
Cisplatin

Figure 3

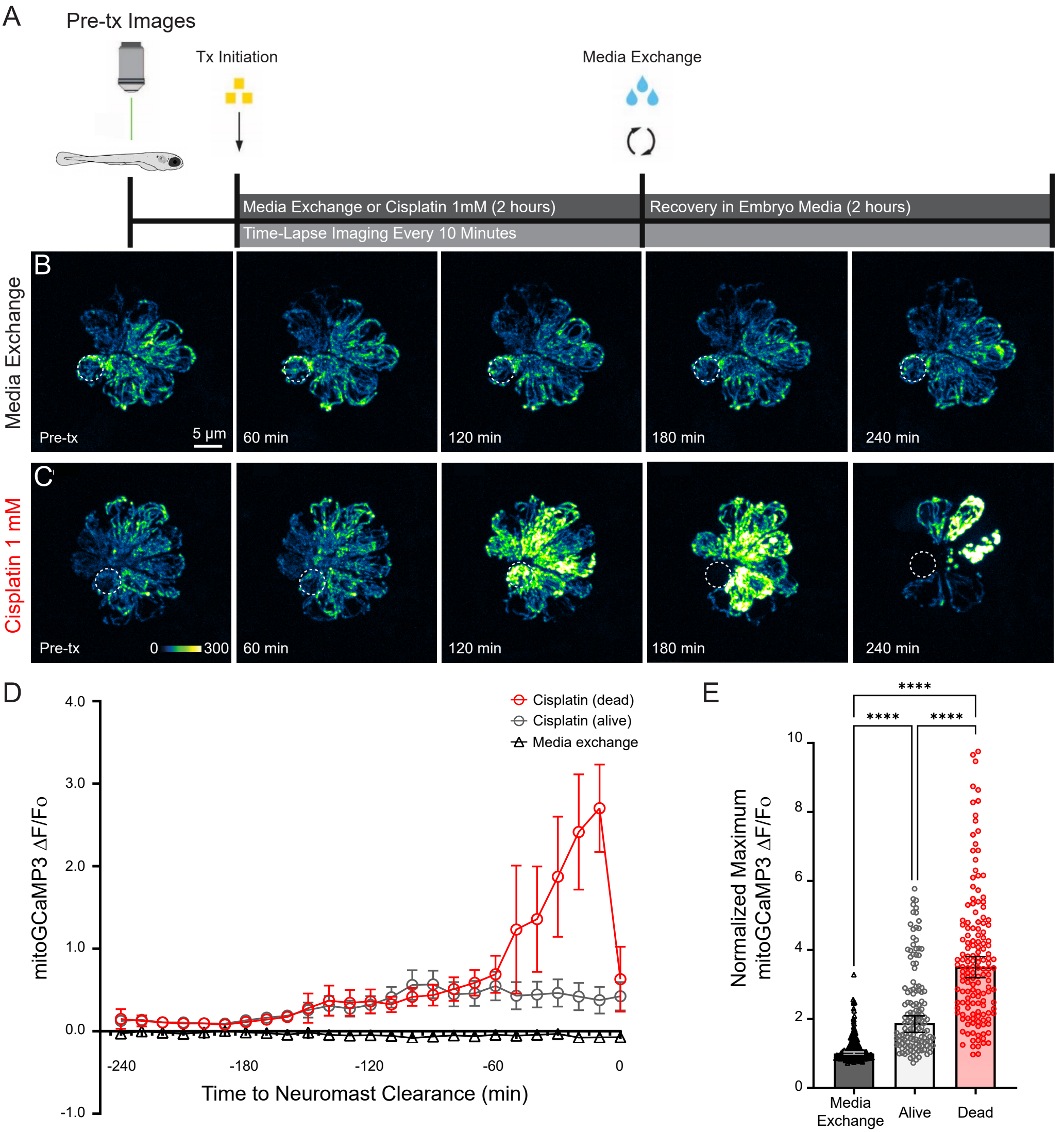
A
Pre-tx Images
Tx Initiation
Media Exchange
Media Exchange or Cisplatin 1mM (2 hours)
Recovery in Embryo Media (2 hours)
Time-Lapse Imaging Every 10 Minutes
B
Media Exchange
Pre-tx
5 µm
60 min
120 min
180 min
240 min
C
Cisplatin 1 mM
Pre-tx
0
300
60 min
120 min
180 min
240 min
D
Cisplatin (dead)
Cisplatin (alive)
Media exchange
mitoGCaMP3 ΔF/Fo
4.0
3.0
2.0
1.0
0.0
-1.0
-240
-180
-120
-60
0
Time to Neuromast Clearance (min)
E
****
****
****
Normalized Maximum mitoGCaMP3 ΔF/Fo
10
8
6
4
2
0
Media Exchange
Alive
Dead

Figure 4

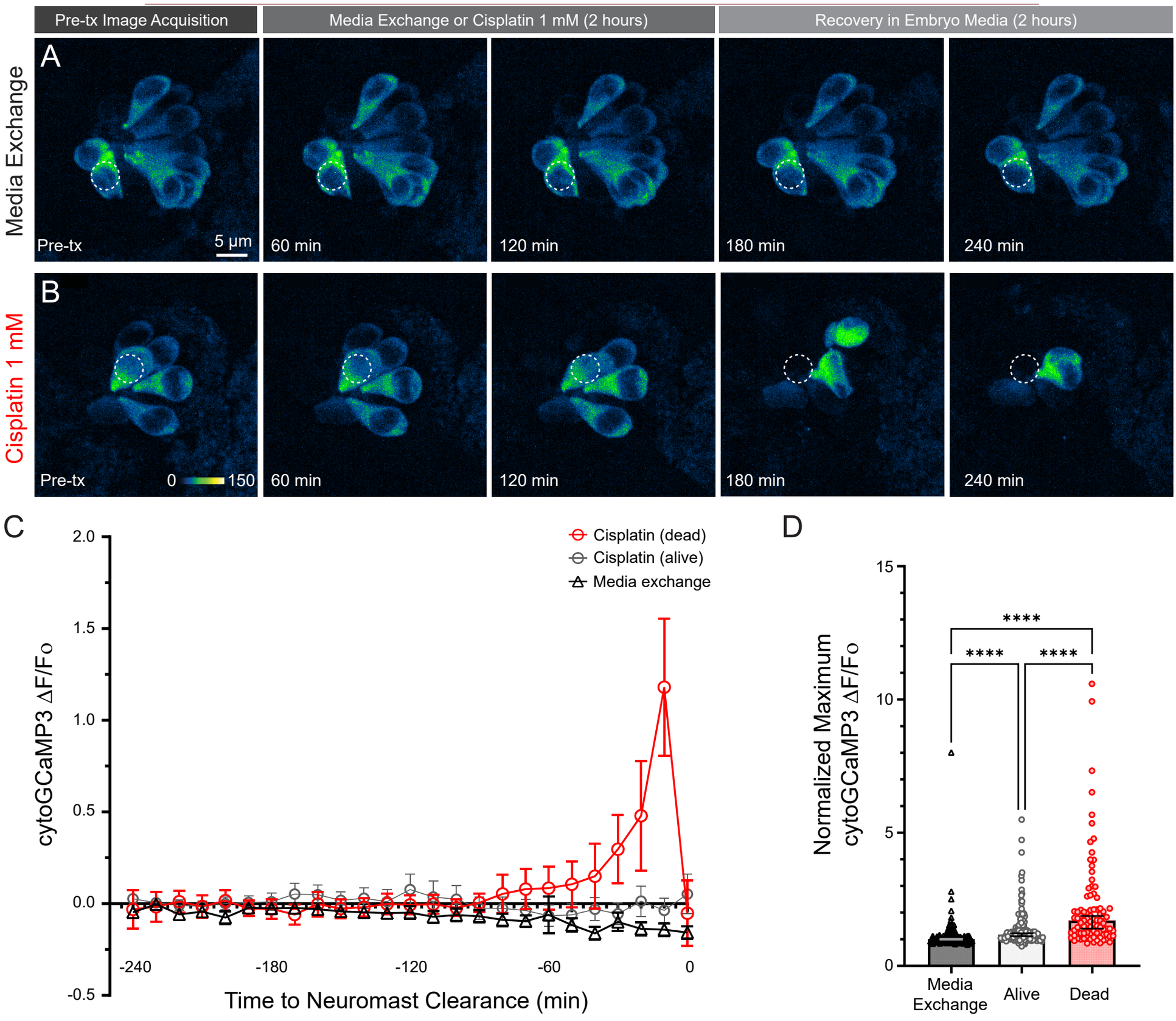
Pre-tx Image Acquisition
Media Exchange or Cisplatin 1 mM (2 hours)
Recovery in Embryo Media (2 hours)
Media Exchange
A
Pre-tx
5 µm
60 min
120 min
180 min
240 min
Cisplatin 1 mM
B
Pre-tx
0
150
60 min
120 min
180 min
240 min
C
Cisplatin (dead)
Cisplatin (alive)
Media exchange
cytoGCaMP3 ΔF/F0
2.0
1.5
1.0
0.5
0.0
-0.5
-240
-180
-120
-60
0
Time to Neuromast Clearance (min)
D
Normalized Maximum cytoGCaMP3 ΔF/F0
15
10
5
0
****
****
****
Media Exchange
Alive
Dead

Figure 5

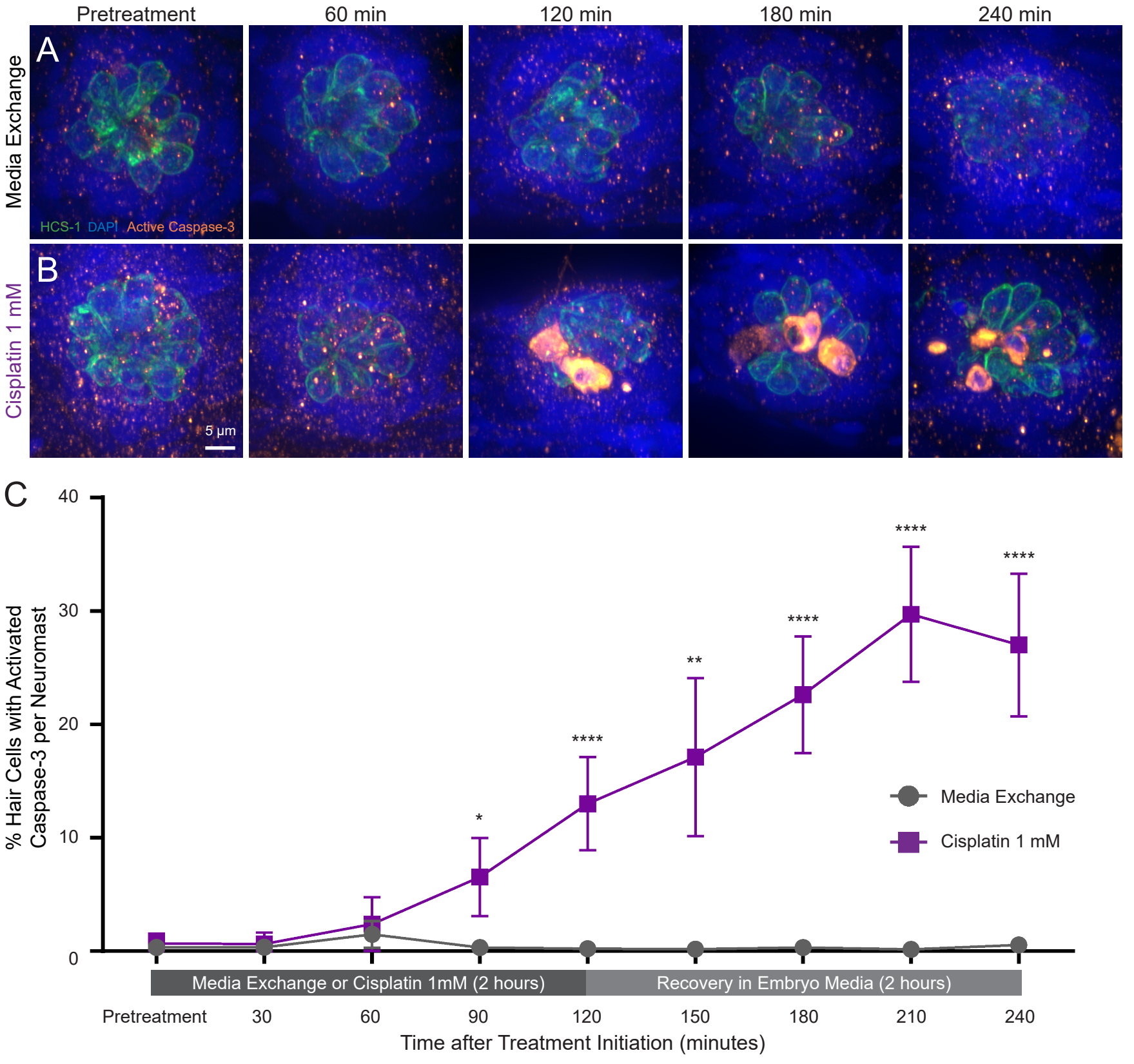
Pretreatment
60 min
120 min
180 min
240 min
Media Exchange
Cisplatin 1 mM
A
B
HCS-1 DAPI Active Caspase-3
5 µm
C
% Hair Cells with Activated Caspase-3 per Neuromast
40
30
20
10
0
*
****
**
****
****
****
Media Exchange
Cisplatin 1 mM
Media Exchange or Cisplatin 1mM (2 hours)
Recovery in Embryo Media (2 hours)
Pretreatment
30
60
90
120
150
180
210
240
Time after Treatment Initiation (minutes)

Figure 6

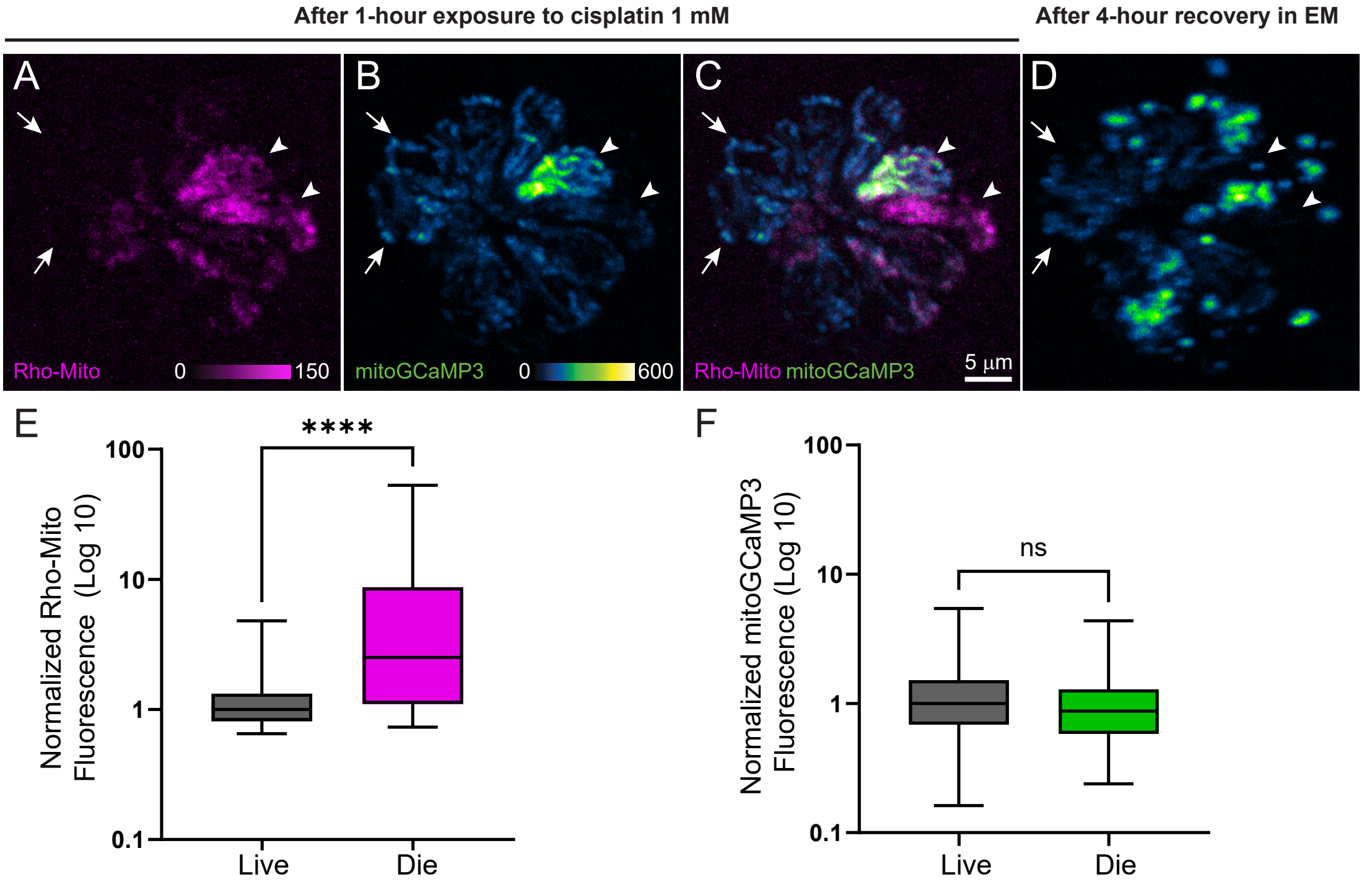
After 1-hour exposure to cisplatin 1 mM
After 4-hour recovery in EM
A
B
C
D
Rho-Mito
0
150
mitoGCaMP3
0
600
Rho-Mito mitoGCaMP3
5 µm
E
****
Normalized Rho-Mito Fluorescence (Log 10)
100
10
1
0.1
Live
Die
F
ns
Normalized mitoGCaMP3 Fluorescence (Log 10)
100
10
1
0.1
Live
Die

Figure 7

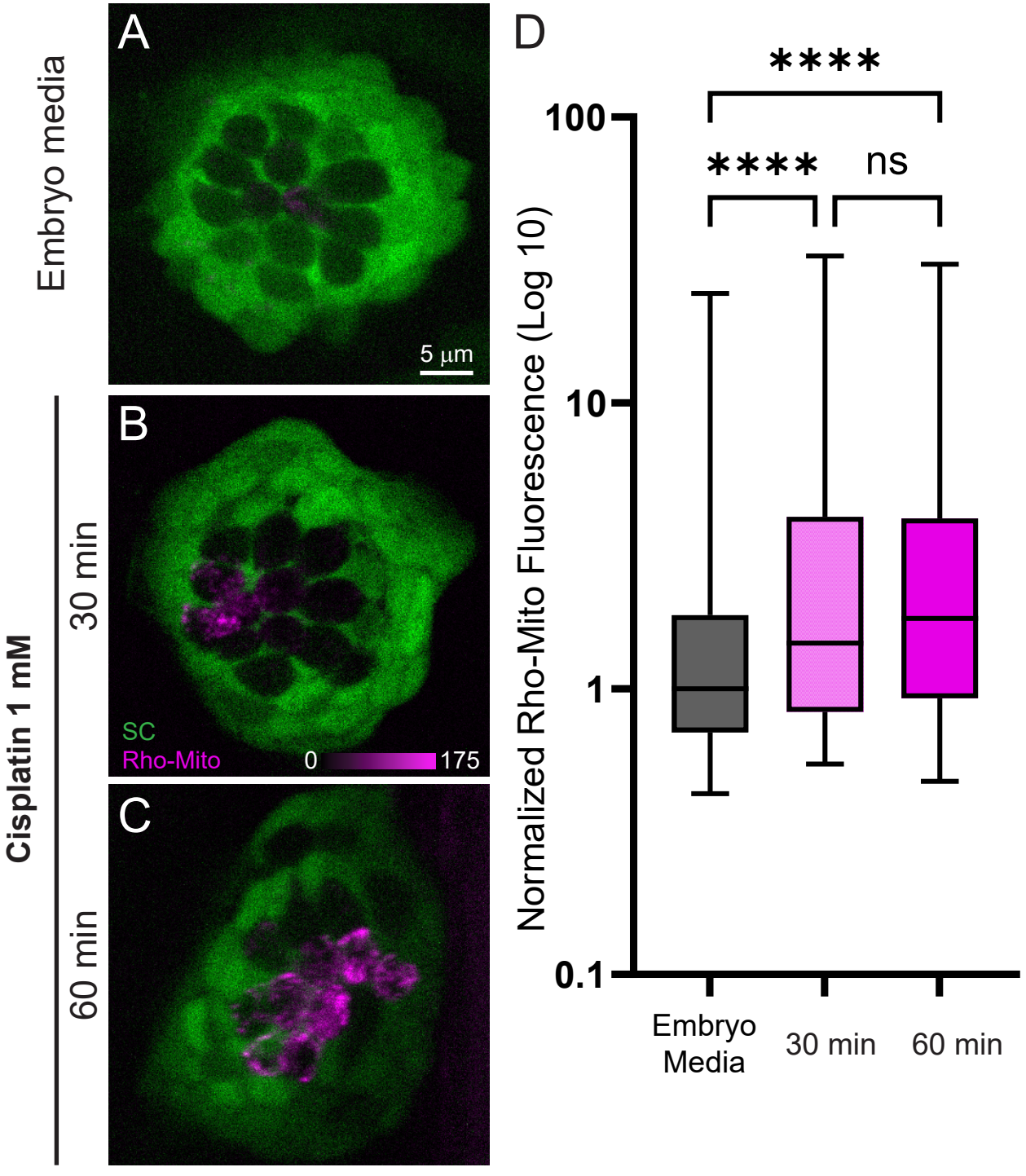
A
Embryo media
5 µm
B
30 min
SC
Rho-Mito
0
175
C
60 min
Cisplatin 1 mM
D
****
****
ns
100
10
1
0.1
Normalized Rho-Mito Fluorescence (Log 10)
Embryo Media
30 min
60 min